Turkish Journal of Chemistry
http://journals.tubitak.gov.tr/chem/
Research Article

Turk J Chem
(2015) 39: 917 – 929

doi:10.3906/kim-1502-73

# Tetraphenylsilane group containing carbazoles as high triplet energy host materials for solution-processable PhOLEDs

**Saliha ÖNER, İlker ÖNER, Haydar AKDAĞ, Canan VARLIKLI***
Ege University, Solar Energy Institute, Bornova, İzmir, Turkey

**Received:** 11.02.2015 • **Accepted/Published Online:** 22.05.2015 • **Printed:** 30.10.2015

**Abstract:** A series of solution processable, wide band-gap host materials composed of carbazole and tetraphenylsilane groups were designed and synthesized. Their thermal, electrochemical, and photophysical properties were fully investigated. The introduction of bulky tetraphenylsilane and *tert*-butyl groups around the carbazole led to high glass transition temperatures ($T_g$) between 120 and 204 °C. The triplet energies ($E_T$) of the synthesized materials were examined by low temperature (77 K) photoluminescence studies and determined as $E_T > 2.6$ for all compounds. Phosphorescent organic light-emitting devices with the ITO/PEDOT:PSS/EML/TPBi/$Cs_2CO_3$/Al device structure were fabricated by using synthesized materials as the host and two kinds of phosphorescent emitters, FIrpic and $Ir(ppy)_3$, as the guests. The highest luminous and power efficiency values obtained by using FIrpic were 3.6 cd $A^{-1}$ and 1.48 lm $W^{-1}$, respectively, with commission International de I'Eclairage (CIE) coordinates of (0.17, 0.36), whereas these values were 7.8 cd $A^{-1}$ and 2.9 lm $W^{-1}$ for the device structure when $Ir(ppy)_3$ was used as the guest [CIE (0.28, 0.62)].

**Key words:** Host material, blue and green PhOLEDs, tetraphenylsilane, carbazole

## 1. Introduction

Phosphorescent organic light emitting diodes (PhOLEDs) have attracted great attention because of their ability to reach nearly 100% internal quantum efficiency by using both singlet (25%) and triplet (75%) excitons.[1–3] In order to prevent triplet–triplet annihilation and concentration quenching, which have hindering effects on device efficiency, phosphorescent emitters should be doped in a suitable host material.[4,5] However, the design of the host material is very important and several requirements should be met: i) the triplet energy of the host material should be higher than that of the phosphorescent emitter to prevent exothermic energy transfer from the emissive dopant to the host material,[6] ii) the glass transition temperature of the host material should be high for good film-forming properties,[7,8] iii) the highest occupied molecular orbital (HOMO) and lowest unoccupied molecular orbital (LUMO) energy levels of the host material and the phosphorescent emitter should be appropriate for efficient energy transfer,[9,10] and iv) the host material should have good charge transporting properties.

A carbazole group containing 4,4′-bis(*n*-carbazolyl)-1,1′-biphenyl (CBP) host material is widely used as the host material for PhOLED applications, but the triplet energy of the CBP ($E_T$ = 2.56 eV) is lower than that of the blue phosphorescent FIrpic ($E_T$ = 2.65 eV), which hampers device efficiency due to back

*Correspondence: canan.varlikli@ege.edu.tr, onerilker@gmail.com

energy transfer.[6] Several studies have been conducted on the modification of CBP for increasing triplet energy and glass transition temperature.[11,12] These studies are mainly focused on decreasing the conjugation between the carbazole groups by creating a twisted structure and/or introduction of a nonconjugated linkage such as diphenylether, tetraphenylsilane, or $sp^3$ hybridized carbon atoms between the molecular entities.[13–19] Among these, tetraphenysilane-based host materials have been widely used in OLED applications because of their high triplet energy and high glass transition temperature.[20,21] The effective interruption of the $\pi$ conjugation with the $\delta$-Si structure ensures a high $E_T$. Moreover, the bulky phenyl groups around the silicon atom increase the molecular weight and steric hindrance, providing high $T_g$ and better film-forming properties. However, most of the previously reported tetraphenysilane derivative host-based PhOLEDs have been fabricated by vacuum deposition method,[16,22,23] which is an expensive technique and not suitable for large area applications. Only a few studies have been reported on solution-processable tetraphenylsilane-based host materials.[18,19,24] Furthermore, efficient, solution-processable, and high triplet energy host materials are still needed to be developed for low cost and simple coating techniques, such as spin coating and inkjet printing.

In this study, we prepared a series of tetraphenylsilane-bridged carbazole compounds named 9,9'-[(diphenylsilanediyl)bis(4,1-phenylene)]bis-9H-carbazole (DiCzSi), 9,9'-[(diphenylsilanediyl)bis(4,1-phenylene)] bis(3,6-di-*tert*-butyl-9H-carbazole) (tBuDiCzSi), 9,9'-[(diphenylsilanediyl)bis(biphenyl-4',4-diyl)]bis-9H-carbazole (DiCzPhSi), and 9,9'-[(diphenylsilanediyl)bis(biphenyl-4',4-diyl)]bis(3,6-di-*tert*-butyl-9H-carbazole) (tBuDiCzPhSi). The combination of carbazole and tetraphenylsilane groups provided relatively high $E_T$ ($>$2.6 eV) and high $T_g$ ($\geq$120 °C). Additionally, good solubility of the synthesized materials in organic solvents allowed their utilization as hosts in solution-processed PhOLEDs. Blue and green light emitting devices are realized by using the synthesized host materials doped with FIrpic and $Ir(ppy)_3$ as the light emitting layer. The highest luminous and power efficiency values obtained by using FIrpic were 3.6 cd $A^{-1}$ and 1.48 lm $W^{-1}$, respectively, whereas these values were 7.8 cd $A^{-1}$ and 2.9 lm $W^{-1}$ for the device structure when $Ir(ppy)_3$ was used as the guest.

## 2. Results and discussion

### 2.1. Synthesis

The synthetic route used to obtain the materials is shown in Scheme Firstly, 9*H*-carbazole (1) was alkylated by using the Friedel–Crafts method and 3,6-di-*tert*-butylcarbazole (2) was obtained. After that, bis(4-bromophenyl)(diphenyl)silane (3) was obtained by Li-halogen exchange reaction by using *n*-BuLi at –78 °C. The Buchwald–Hartwig amination reaction of carbazole and 3,6-di-*tert*-butylcarbazole with molecule 3 in the presence of $Pd(OAc)_2$, $P(t\text{-}Bu)_3$, and $K_2CO_3$ allowed us to obtain the target molecules DiCzSi and tBuDiCzSi. After that, both 9*H*-carbazole and 3,6-di-*tert*-butylcarbazole were reacted with 1-bromo-4-iodobenzene by Ullmann coupling in the presence of Cu, 18-crown-6, and $K_2CO_3$. The brominated derivatives (4 and 5) were then converted to boronic acids (6 and 7) by using *n*-BuLi and $B(OMe)_3$. The Suzuki–Miyaura coupling reaction between the boronic acids and molecule 3 allowed us to obtain the target molecules DiCzPhSi and tBuDiCzPhSi. The molecular structures of the intermediates and the target molecules were confirmed by FTIR, $^1$H NMR, and $^{13}$C NMR spectroscopy and the results were in good agreement with the proposed structures. Details of the synthetic routes followed are given in the supplementary (S) section together with the corresponding structural characterization spectra (Figures S1–S13; on the journal's website).

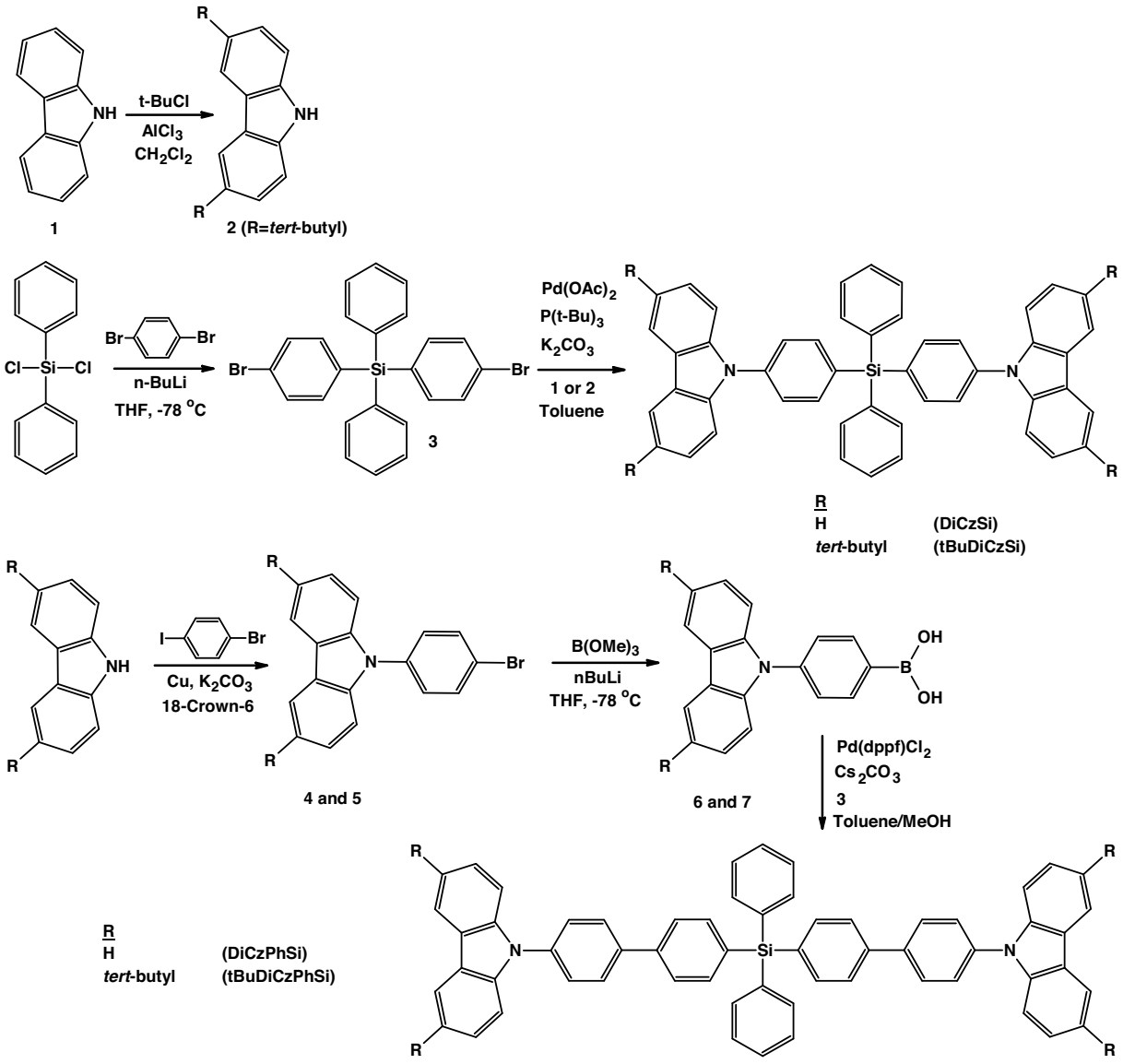


**Scheme.** Molecular structures and the synthetic route for the synthesized materials.

### 2.2. DSC measurements

The thermal properties of the compounds were studied by differential scanning calorimetry (DSC) measurements. The first heating scan of the DSC thermograms revealed the melting points ($T_m$) of the compounds (Figure 1a). $T_m$ values of DiCzSi and DiCzPhSi were determined as 290 °C and 285 °C, respectively. The introduction of *tert*-butyl groups to 3- and 6- positions of the carbazole greatly increased the melting point to 384 °C for tBuDiCzSi and no melting point was observed for tBuDiCzPhSi within the measurement scale (30–400 °C). During the second heating scan (Figure 1b), weak endothermic transitions were observed, indicating the $T_g$ of the compounds, which increased with the increasing molecular weight. Among the compounds, DiCzSi has the lowest $T_g$ (120 °C), which is still much higher than that of the commonly used host material CBP ($T_g$ = 62 °C).[25] Introduction of the diphenylsilane group into the CBP molecule greatly enhanced the $T_g$, which

indicates the positive effect of the nonplanar silicon moiety. Furthermore, the introduction of *tert*-butyl and phenyl groups increased the $T_g$ from 120 °C up to 204 °C. With the increasing temperature, crystallization was observed for DiCzSi and tBuDiCzSi, showing that they have both crystalline and amorphous states. The $T_g$ of the tBuDiCzPhSi was determined as 337 °C, and no other phase transitions could be detected up to 400 °C; therefore, the compound stays in amorphous state. The results showed that all of the synthesized materials have high thermal stability, which is favorable for obtaining smooth and stable films.[19]

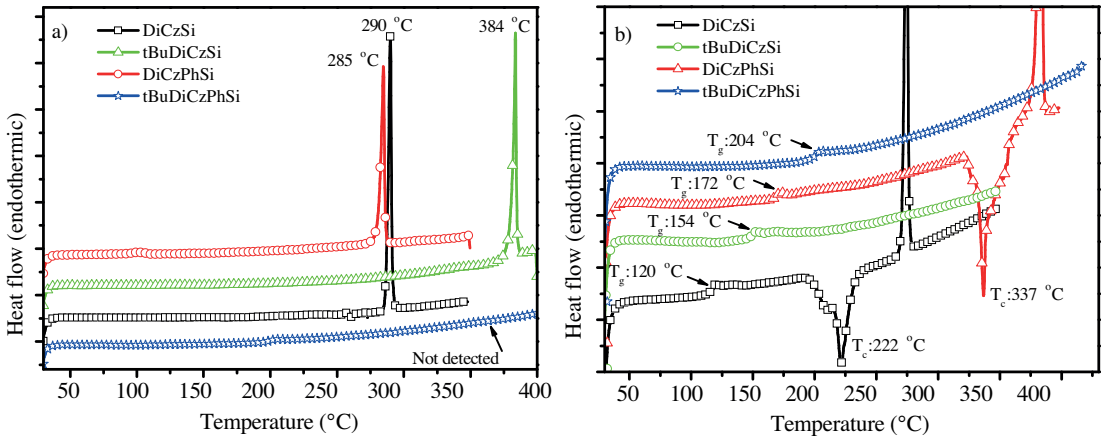


**Figure 1.** a) The first heating scan of the DSC thermograms, which shows the melting points of the compounds, b) the second heating scan of the DSC thermograms, which shows the glass transition ($T_g$) and crystallization temperatures ($T_c$) for the synthesized compounds.

### 2.3. Absorption–photoluminescence studies

The UV-Vis absorption and PL spectra of the compounds were measured in different solvents with different polarities (Figure 2). The maximum absorption peak at around 290 nm is identical for all compounds and can be assigned to the carbazole-centered n–$\pi$* transition and the absorption band between 310 and 350 nm is attributed to the $\pi$–$\pi$* transition of the entire conjugated system.[26] The optical band-gap [$E_{g(opt)}$] of the compounds was calculated from the onset of the UV-Vis absorption spectra, which is around 3.5 eV.

The PL spectra of DiCzSi and tBuDiCzSi are almost identical in $CHCl_3$ solvent, except that the introduction of the *tert*-butyl groups caused a red-shift of 7 nm for the latter. The PL spectrum of DiCzPhSi showed a significant red-shift (ca. 33 nm/in $CHCl_3$ solvent) compared to the DiCzSi counterpart, which is attributed to the extended $\pi$ conjugation between the carbazole and tetraphenylsilane units. The PL spectrum of tBuDiCzPhSi also showed a red-shift (ca. 18 nm/in $CHCl_3$ solvent) compared to the DiCzPhSi counterpart, which is caused by the introduction of the electron-donating *tert*-butyl groups. There was no significant difference between the absorption spectra of the compounds, probably because the molecules were exposed to the same local environment in the ground and excited states. In contrast, the PL maxima of DiCzPhSi and tBuDiCzPhSi showed a bathocromic shift with increasing solvent polarity (Figure 2). Actually, this was expected as the $\pi$ character in those two compounds is dominant and therefore a solvent polarity increase would have a dramatic effect on the $\pi$*–$\pi$ relaxation. A summary of the photophysical data is given in Table 1.

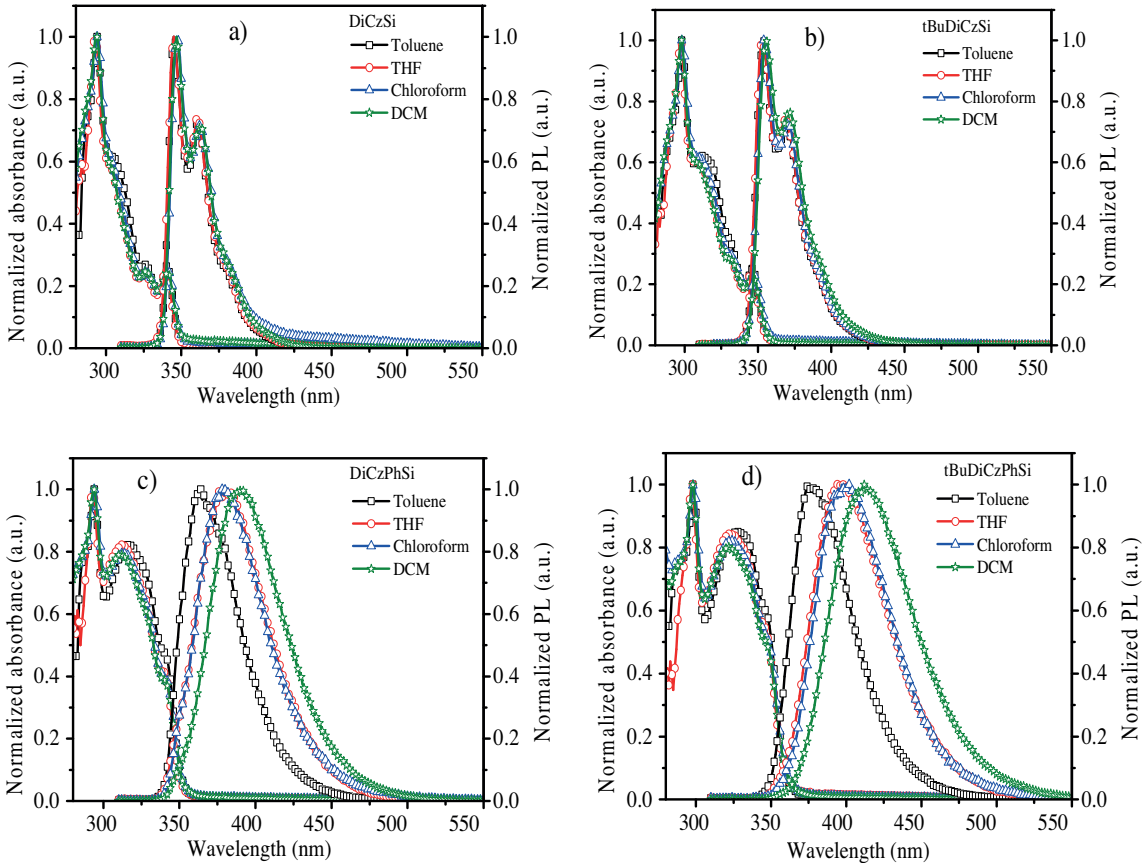


**Figure 2.** UV-Vis and PL spectra of the synthesized compounds, a) DiCzSi, b) tBuDiCzSi, c) DiCzPhSi, d) tBuDiCzPhSi obtained in different solvents ($10^{-5}$ M), at room temperature.

**Table 1.** Physical, optical and electrochemical data for the synthesized compounds.

| Host material | Tm/Tg/Tc[a] (°C) | $\lambda_{abs}$ [b] (nm) | $\lambda^{b}_{PL}$ (nm) | $E_T$ [c] (eV) | $E_{ox}$ [d] (V) | HOMO[e] (eV) | LUMO[e] (eV) | $E_{g(opt)}$ [f] (eV) |
|---|---|---|---|---|---|---|---|---|
| DiCzSi | 290/120/222 | 294, 306, 326, 341 | 347, 362 | 3.00 | 1.18 | –5.69 | –2.15 | 3.54 |
| tBuDiCzSi | 384/172/337 | 298, 312, 332, 347 | 354, 370 | 3.00 | 1.06 | –5.57 | –2.10 | 3.47 |
| DiCzPhSi | 285/154/NA | 294, 314 | 380 | 2.64 | 1.16 | –5.67 | –2.15 | 3.52 |
| tBuDiCzPhSi | NA/204/NA | 298, 324 | 398 | 2.64 | 1.06 | –5.57 | –2.12 | 3.45 |

[a] $T_m/T_g/T_c$ were obtained from the DSC measurements (10 °C $min^{-1}$ $N_2$ gas flow), [b] maximum absorption and PL wavelengths were measured in $CHCl_3$ solution ($10^{-5}$ M), [c] triplet energy values were calculated from the maximum wavelength of the phosphorescence spectra measured in DCM at 77 K, [d] oxidation potentials were determined from the onset of the CV curves, e) HOMO energy levels were calculated from the onset of the oxidation potentials, [e] LUMO energy levels were deduced from the formula LUMO = HOMO + $E_{g(opt)}$, [f] $E_{g(opt)}$ were calculated from the onset of the absorption spectra in $CHCl_3$ solution.

The phosphorescence spectra of the materials were determined by low temperature (77 K) PL measurements in dichloromethane (DCM) ($10^{-5}$ M solutions). DiCzSi and tBuDiCzSi showed a new emission band with a maximum peak at around 415 nm, and the emission maximum shifted to ∼470 nm for DiCzPhSi and

tBuDiCzPhSi (Figure 3). The $E_T$ values were estimated to be >2.6 eV by taking the highest-energy peak of phosphorescence as the transition energy of $T_1 \rightarrow S_0$, which corresponded to the vibronic 0–0 transition between these two electronic states.[19,27] The $E_T$ values of DiCzSi and tBuDiCzSi were calculated as 3.0 eV. This value is higher than that of the blue phosphorescent emitter FIrpic ($E_T$ = 2.65 eV); this meant that they are suitable hosts for effectively confining the excitons on FIrpic dopant.[6] The addition of the –phenyl ring between the carbazole and tetraphenysilane groups caused a significant red-shift (ca. 54 nm) because of the extension of the $\pi$ conjugation, resulting in lower triplet energy for DiCzPhSi and tBuDiCzPhSi ($E_T$ = 2.64 eV), which is close to the triplet energy of the green phosphorescent emitter $Ir(ppy)_3$ ($E_T$ = 2.4 eV).[4] Because of their suitable $E_T$ values, all synthesized host materials were used with the green emitter $Ir(ppy)_3$, and the higher triplet energy host materials, DiCzSi and tBuDiCzSi, were used with the blue emitter FIrpic.

### 2.4. Electrochemical studies

The electrochemical behaviors of the compounds were determined by cyclic voltammetry (CV). All of the synthesized compounds showed reversible and/or nonreversible oxidation peaks because of the *p*-type carbazole groups, and no reduction peak within the electrochemical window (+2/–2 V) was detected. With regard to the energy level of the ferrocene reference (4.8 eV relative to the vacuum level), the HOMO energy levels were calculated by using the equation of $E_{HOMO} = -e\,(4.8 + E_{(ox)} - E_{(Fc)})$, in which $E_{ox}$ was taken from the onset of the oxidation potential.[28] As shown in Figure 4, tBuDiCzSi and tBuDiCzPhSi showed $E_{ox}$ values of around 1.06 V that correspond to a HOMO energy level of –5.57 eV. DiCzSi and DiCzPhSi exhibited a nonreversible oxidation peak because of the instability of the radical cations of these carbazoles since the electro-active -3 and -6 positions may have undergone dimerization under the CV scan.[29,30] The $E_{ox}$ values were around 1.2 V and HOMO energy levels were calculated as –5.69 eV and –5.67 eV for DiCzSi and DiCzPhSi, respectively.

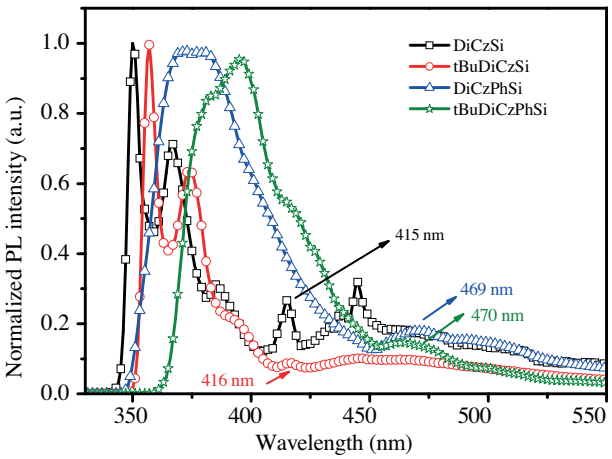


**Figure 3.** Phosphorescence spectra of the synthesized materials recorded at 77 K in $CHCl_3$ ($10^{-5}$ M).

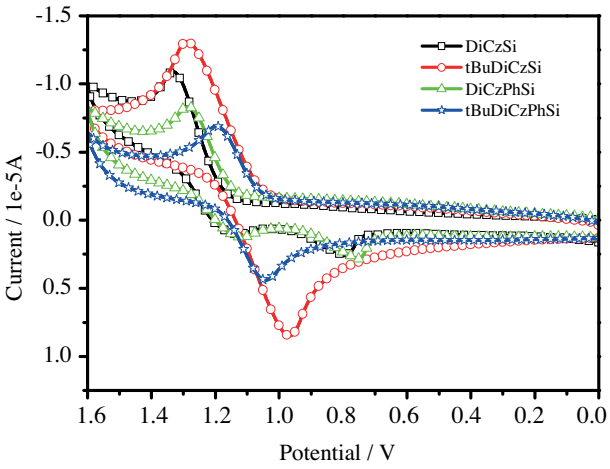


**Figure 4.** Cyclic voltammograms of the synthesized materials measured in $CHCl_3$.

CV studies are also important to determine the electrochemical stability of the synthesized compounds,[31,32] which has a significant importance in terms of device efficiency.[33] The consecutive CV scans (20 cycles) revealed that the *tert*-butyl group containing tBuDiCzSi and tBuDiCzPhSi were electrochemically stable and there was no new wave formation after continuous cycling (Figure S13; on the journal's website). However, during the

consecutive CV scans of DiCzSi and DiCzPhSi, the oxidation peak at around 1.2 eV disappeared and a new wave at around 0.8 eV appeared, due to the oxidation of the carbazole groups.[34] The LUMO energy levels were obtained by using the following equation: LUMO = HOMO + $E_{g(opt.)}$, which was around –2.10 eV for all compounds. The electrochemical data are summarized in Table 1.

### 2.5. Theoretical calculations

In order to understand the electronic states of the host molecules, density functionalized theory (DFT) calculations were performed by using Gaussian 09 C.01 software.[35] The geometry optimizations and frequency calculations were performed at the level of B3LYP/ cc-pVDZ (any imaginary frequency). Calculated energy values of density surfaces of the HOMO and LUMO are shown in Figure 5 and Table 2. The triplet energy ($E_T$) of the compounds was calculated using time-dependent density functional theory (TD-DFT). The results revealed that the HOMO and LUMO electron density distributions of the synthesized materials are mainly localized on the carbazole and tetraphenylsilane fragments, respectively.[36] As shown in Figure 5, the highly twisted configurations of the host molecules allow the separation of HOMO and LUMO, which is favorable for the efficient hole and electron transporting properties.[37] The calculated triplet energy levels were around 3.1 eV for the DiCzSi and tBuDiCzSi, which was consistent with the experimental results (3.0 eV). The $E_T$ of the DiCzPhSi and tBuDiCzPhSi were calculated as 3.03 eV and 2.98 eV, respectively.

**Table 2.** Calculated energy values of the host materials.

| Host material | HOMO (eV) | LUMO (eV) | $E_g$ (eV) | $S_1$ (eV) | $E_T$ (eV) |
|---|---|---|---|---|---|
| DiCzSi | –5.55 | –1.44 | 4.11 | 3.83 | 3.15 |
| tBuDiCzSi | –5.34 | –1.05 | 4.29 | 3.73 | 3.10 |
| DiCzPhSi | –5.52 | –1.45 | 4.07 | 3.56 | 3.03 |
| tBuDiCzPhSi | –5.31 | –1.40 | 3.91 | 3.44 | 2.98 |

### 2.6. PhOLED performances

To evaluate the EL properties of the synthesized compounds as solution-processable host materials, we fabricated blue and green PhOLEDs with the configuration of ITO/PEDOT:PSS (40 nm)/B-EML (or G-EML) (70 nm)/TPBi (20 nm)/$Cs_2CO_3$ (3 nm)/Al (100 nm), where B-EML and G-EML refer to the synthesized host materials doped with FIrpic and $Ir(ppy)_3$, respectively. The device architectures are listed in Table 3. The optimized doping concentrations of FIrpic and $Ir(ppy)_3$ were 15 wt.% and 10 wt.%, respectively.

**Table 3.** Device names and corresponding structures.

| Device name | Structures |
|---|---|
| Device B1 | ITO/PEDOT:PSS/DiCzSi:FIrpic/TPBi/$Cs_2CO_3$/Al |
| Device B2 | ITO/PEDOT:PSS/tBuDiCzSi:FIrpic/TPBi/$Cs_2CO_3$/Al |
| Device G1 | ITO/PEDOT:PSS/DiCzSi:$Ir(ppy)_3$/TPBi/$Cs_2CO_3$/Al |
| Device G2 | ITO/PEDOT:PSS/tBuDiCzSi:$Ir(ppy)_3$/TPBi/$Cs_2CO_3$/Al |
| Device G3 | ITO/PEDOT:PSS/DiCzPhSi:$Ir(ppy)_3$/TPBi/$Cs_2CO_3$/Al |
| Device G4 | ITO/PEDOT:PSS/tBuDiCzPhSi:$Ir(ppy)_3$/TPBi/$Cs_2CO_3$/Al |

Figure 6 depicts the luminance–voltage–current density (L–V–J) characteristics of blue (devices B1–B2) and green (devices G1–G4) emitting devices. The turn-on voltages of devices were between 5 and 8 V (taking

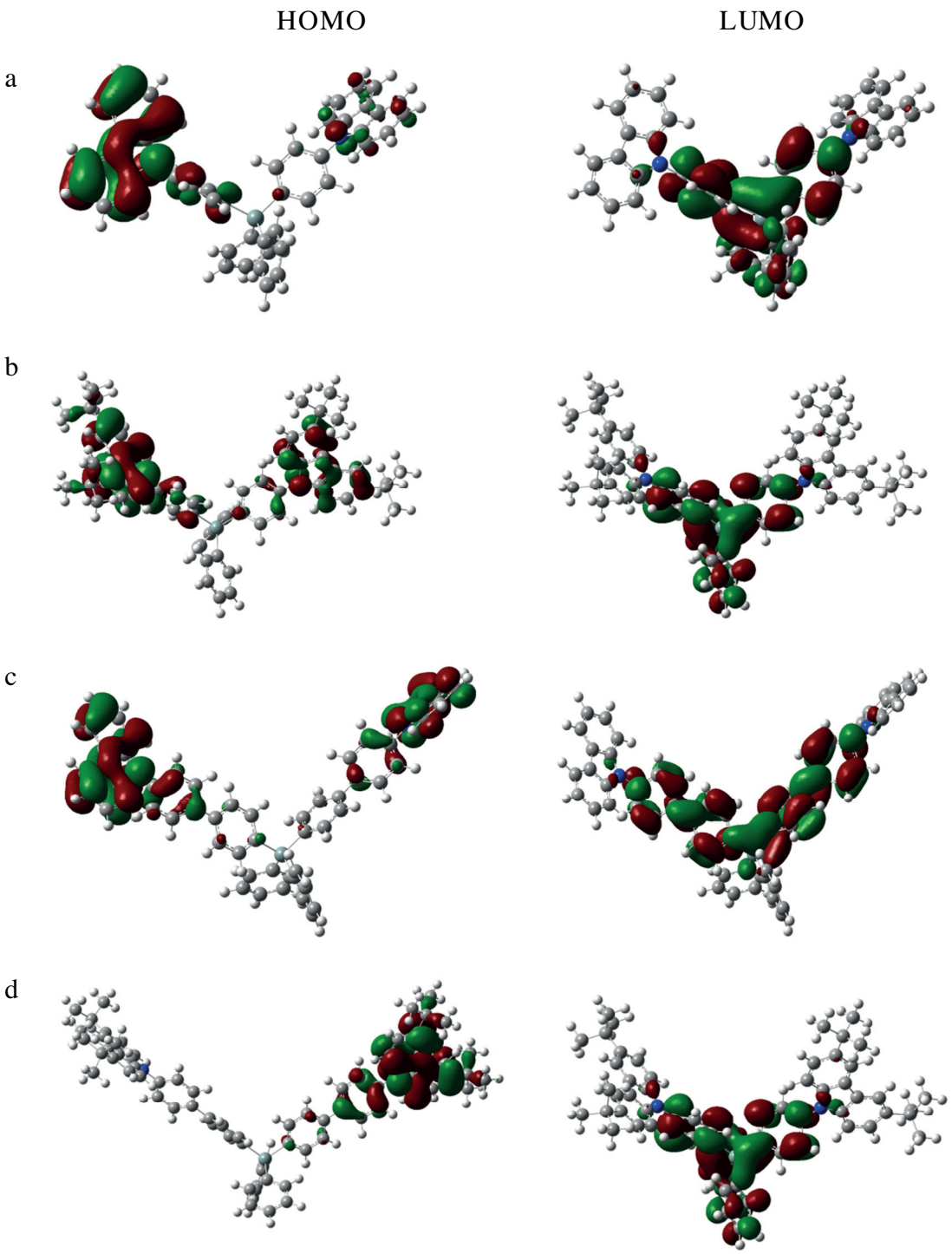


**Figure 5.** Calculated density surfaces of the molecular orbitals of a) DiCzSi, b) tBuDiCzSi, c) DiCzPhSi, and d) tBuDiCzPhSi.

1 cd $m^{-2}$ to be the turn-on standard). Among the blue devices, the rise in the current density of device B1 might be due to a better hole or electron transport within the emitting layer, resulting in lower turn-on voltage. The same phenomenon was also observed for green devices. The devices with nonsubstituted host materials (B1, G1, G3) showed higher driving voltages than those of the *tert*-butyl substituted derivatives (B2, G2, G4).

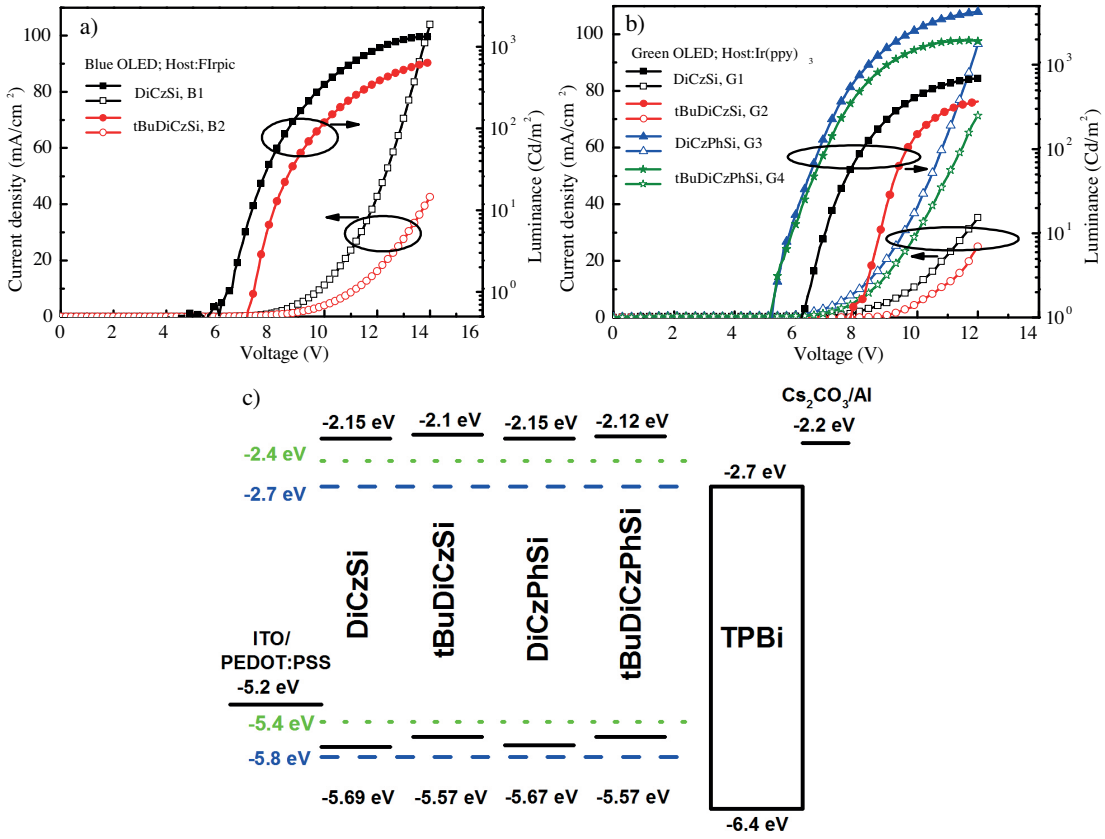


**Figure 6.** The luminance–voltage–current density ($L$–$V$–$J$) characteristics for a) blue PhOLEDs and b) green PhOLEDs. The symbols apply for luminance (filled) and current density (hollow) of the devices. c) Energy level diagram of the PhOLEDs, the dashed and dotted lines apply for FIrpic and $Ir(ppy)_3$, respectively.

The luminous and power efficiency versus current density of blue and green PhOLEDs is shown in Figure 7. Among the blue emitting devices, device B1, which contains DiCzSi as the host material, showed higher luminous and power efficiency than did device B2, which contains *tert*-butyl substituted derivative (tBuDiCzSi). Device B1 exhibited the highest luminous efficiency of 3.6 cd $A^{-1}$, the highest power efficiency of 1.48 lm $W^{-1}$, and a maximum brightness of 1324 cd $m^{-2}$. These results are in good agreement with the data reported by Hu et al.[22] On the other hand, for green PhOLEDs, device G3 showed higher luminous and power efficiency than did the other devices, with a maximum luminous efficiency of 7.8 cd $A^{-1}$, maximum power efficiency of 2.9 lm $W^{-1}$, and maximum brightness of 4237 cd $m^{-2}$. The EL performances of the devices are summarized in Table 4. Although the introduction of *tert*-butyl groups increased the $T_g$, electrochemical stability, and solubility of the synthesized compounds, the OLED devices with *tert*-butyl group containing host materials resulted in lower device efficiencies. The lower efficiency may be attributed to the constrained charge transport caused by the insulating effect of the *tert*-butyl groups.[38]

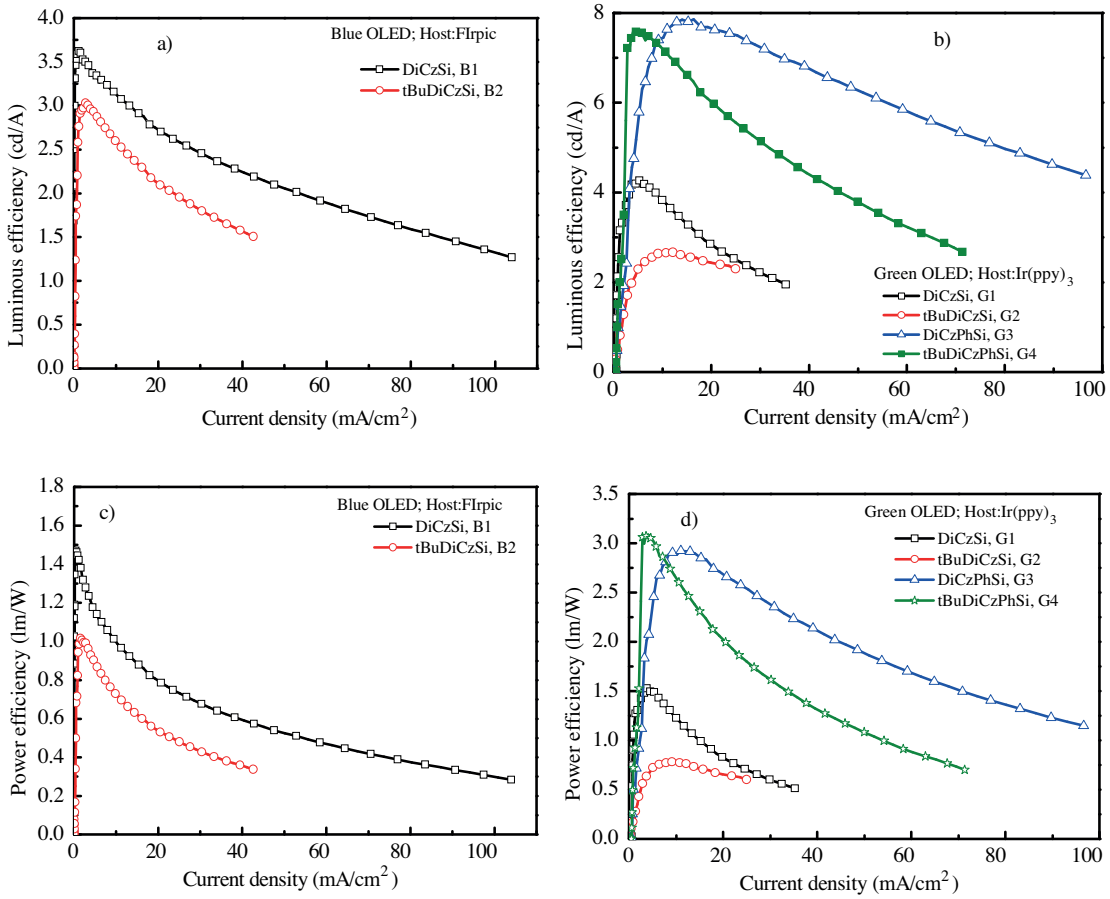


**Figure 7.** Luminous efficiency (a,b) and power efficiency (c,d) versus current density characteristics for blue and green OLEDs.

**Table 4.** Maximum luminance, current, power, EQE efficiencies and CIE color coordinates of blue devices B1 and B2, and green devices G1–G4.

| Device name | $V_{on}^{a}$ (V) | Max. luminance (cd/m$^2$) | Max. current efficiency (cd/A) | Max. power efficiency (lm/W) | Max. EQE (%) | CIE (x, y) (@ 10 V) |
|---|---|---|---|---|---|---|
| B1 | 6.4 | 1324 | 3.6 | 1.48 | 1.72 | 0.17, 0.36 |
| B2 | 7.3 | 642 | 3 | 1 | 1.47 | 0.17, 0.34 |
| G1 | 6.2 | 689 | 4.27 | 1.5 | 1.26 | 0.28, 0.62 |
| G2 | 7.8 | 367 | 2.65 | 0.78 | 0.8 | 0.27, 0.62 |
| G3 | 5.2 | 4237 | 7.8 | 2.9 | 2.27 | 0.28, 0.62 |
| G4 | 5.2 | 1950 | 7.6 | 3 | 2.26 | 0.28, 0.62 |

[a] Turn-on voltage

Electroluminescence (EL) spectra of the blue and green devices at 12 V are presented in Figure 8. All of the devices showed blue and green emission spectra peaking at 475 nm and 510 nm, which originated from the emission of FIrpic and $Ir(ppy)_3$, respectively, implying efficient energy transfer from host materials to dopant molecules.

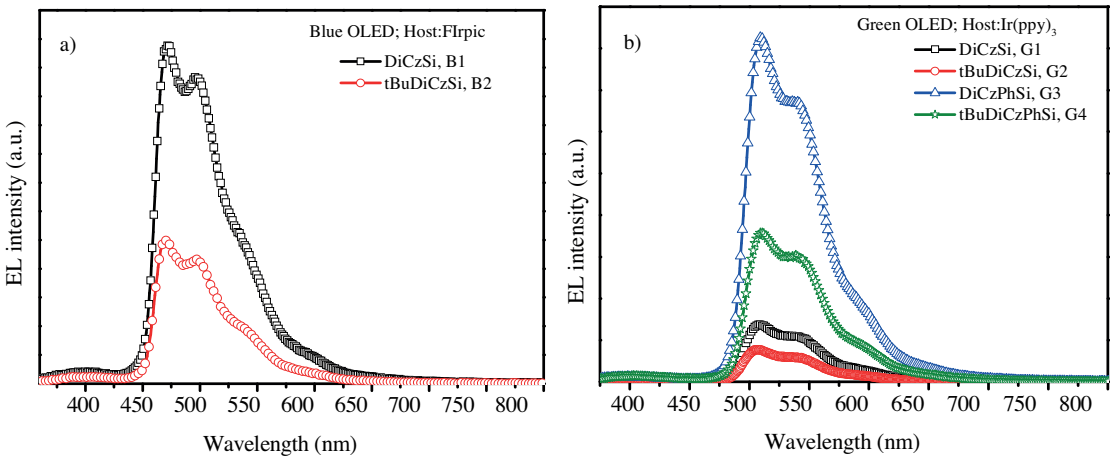


**Figure 8.** Electroluminescence spectra of a) blue and b) green devices at 12 V.

In summary, a series of tetraphenylsilane-bridged carbazole-based host molecules, DiCzSi, tBuDiCzSi, DiCzPhSi, and tBuDiCzPhSi, were synthesized and characterized. The high glass transition temperature ($\geq$120 °C) and high triplet energy (>2.6 eV) host materials were used for blue and green PhOLEDs.

By using DiCzSi:FIrpic as the emissive layer (blue PhOLED, color coordinates (0.17, 0.36)), the highest luminous and power efficiency values of 3.6 cd $A^{-1}$ and 1.48 lm $W^{-1}$, respectively, were obtained. Among the green PhOLEDs, the DiCzPhSi:Ir(ppy)$_3$-based device demonstrated the best performance, with a maximum brightness of 4200 cd $m^{-2}$ at 12 V and a maximum luminous efficiency of 7.8 cd $A^{-1}$ at 8 V with the color coordinates of (0.28, 0.62). The higher efficiencies for the devices with DiCzPhSi:Ir(ppy)$_3$ and tBuDiCzPhSi:Ir(ppy)$_3$ emissive layers can be attributed to the good triplet energy level match between guest and host.

## 3. Experimental

### 3.1. Materials and instruments

Solvents were carefully dried and distilled from appropriate drying agents prior to use. All reactions were performed under a dry nitrogen atmosphere. Commercially available reagents were supplied from Aldrich and used without further purification. Poly(3,4-ethylenedioxythiophene):poly(styrene sulfonate) (PEDOT:PSS) was purchased from Ossila Company. Cesium carbonate ($Cs_2CO_3$), 2,2′,2″-(1,3,5-benzinetriyl)-tris(1-phenyl-1-*H*-benzimidazole) (TPBi), and *fac*-tris(2-phenylpyridine)iridium(III) [Ir(ppy)$_3$] were provided by Aldrich. Iridium(III)bis[(4,6-difluorophenyl)-pyridinato-N,C$^{2\prime}$]picolinate [FIrpic] was purchased from ADS Dyes. Tetrabutyl ammonium hexafluorophosphate ($TBAPF_6$) was purchased from Fluka. Indium tin oxide (ITO) glass substrates with a sheet resistance of 9–15 Ω $sq^{-1}$ were provided by LumTec.

$^1$H NMR and $^{13}$C NMR spectra were measured on a Bruker 400 MHz spectrometer using tetramethylsilane (TMS) as an internal standard. The infrared (IR) spectra were obtained by using a PerkinElmer Spectrum BX-FTIR spectrophotometer. FAB-MASS measurements were carried out on a Finnigan MAT 95 mass spectrometer. UV-Vis, photoluminescence (PL), and phosphorescence emission spectra (77 K) were recorded by using Lambda 950 UV-Vis-NIR and FLS920P spectrophotometers, respectively. Electrochemical studies were carried out with a CH Instrument 660 B Model Electrochemical Workstation by using a three-electrode electrochemical cell configuration consisting of a glassy carbon working electrode, Pt wire auxiliary electrode, and a Ag wire reference electrode with ferrocene/ferrocenium ($CP_2Fe/CP_2Fe^+$) as the internal standard, and 0.1

M $TBAPF_6$ in $CHCl_3$ was used as the supporting electrolyte. Cyclic voltammograms were obtained at a scan rate of 100 mV $s^{-1}$ and the oxidation potentials ($E_{ox}$) were determined from the onsets of the oxidation peaks.

Thermal properties of the materials were analyzed by the use of a PerkinElmer Pyris 6 DSC instrument. The heating rate was 10 °C $min^{-1}$ and the nitrogen flow rate was 10 mL $min^{-1}$. Solution-processed coatings were prepared using a Laurell WS-400B-6NPP-LITE spin coater. Film thicknesses were measured using an Ambios XP-1 high-resolution surface profiler. Electron transport layer and metal depositions were performed with a shadow mask using a vacuum evaporator attached to an MBRAUN 200B glovebox system. The EL spectra and L–V–J curves were obtained using a Keithley 2400 source measurement unit and calibrated Hamamatsu C9920-12 External Quantum Efficiency (EQE) measurement system.

### 3.2. Device fabrication and measurement

The OLEDs were fabricated in a structure of indium–tin oxide (ITO)/PEDOT:PSS (40 nm)/emissive layer (80 nm)/TPBi (20 nm)/$Cs_2CO_3$ (3 nm)/Al (200 nm). Prior to organic layer deposition, the ITO substrates were cleaned with acetone and isopropanol ultrasonically for 15 min. For all devices, PEDOT:PSS was firstly spin-coated onto ITO glass substrates as first layer and annealed in a vacuum oven at 120 °C for 30 min to form a 40-nm film. Following this, the materials for the emission layer were dissolved in chlorobenzene at a stock density of 10 mg $mL^{-1}$ (at various doping weight percentages, wt%) and were spin-coated onto the PEDOT:PSS layer. A 20-nm-thick TPBi was vacuum-deposited on top of the EML at a deposition rate of 0.5 Å $s^{-1}$. Finally, $Cs_2CO_3$ (3 nm) and Al (200 nm) were deposited onto the emitting layer as cathode by thermal evaporation under a vacuum of $1 \times 10^{-6}$ mbar. The emission areas of the devices were 6 $mm^2$.

### Acknowledgments

This work was supported by the Scientific and Technological Research Council of Turkey (TÜBİTAK) (Project #: 113Z253). The authors would like to thank Dr Armağan Kınal for productive discussions on the numerical calculations, which were performed at TÜBİTAK ULAKBİM, High Performance and Grid Computing Center (TRUBA Resources).

The authors are grateful to Prof Dr Sıddık İçli, who retired from Ege University Solar Energy Institute (EU-SEI) in 2014 and made valuable contributions to the organic electronics research infrastructure of EU-SEI.

## References

1. Adachi, C.; Kwong, R. C.; Djurovich, P.; Adamovich, V.; Baldo, M. A.; Thompson, M. E.; Forrest, S. R. *Appl. Phys. Lett.* **2001**, *79*, 2082–2084.
2. Baldo, M. A.; O'Brien, D. F.; You, Y.; Shoustikov, A.; Sibley, S.; Thompson, M. E.; Forrest, S. R. *Nature* **1998**, *395*, 151–154.
3. Baldo, M. A.; Lamansky, S.; Burrows, P. E.; Thompson, M. E.; Forrest, S. R. *Appl. Phys. Lett.* **1999**, *75*, 4–6.
4. Baldo, M.; Adachi, C.; Forrest, S. *Phys. Rev. B* **2000**, *62*, 10967–10977.
5. Baldo, M. A.; Thompson, M. E.; Forrest, S. R. *Nature* **2000**, *403*, 750–753.
6. Holmes, R. J.; Forrest, S. R.; Tung, Y. J.; Kwong, R. C.; Brown, J. J.; Garon, S.; Thompson, M. E. *Appl. Phys. Lett.* **2003**, *82*, 2422–2424.
7. Tsai, M. H.; Lin, H. W.; Su, H. C.; Ke, T. H.; Wu, C. C.; Fang, F. C.; Liao, Y. L.; Wong, K. T.; Wu, C. I. *Adv. Mater.* **2006**, *18*, 1216–1220.

8. Wu, M. F.; Yeh, S. J.; Chen, C. T.; Murayama, H.; Tsuboi, T.; Li, W. S.; Chao, I.; Liu, S. W.; Wang, J. K. *Adv. Funct. Mater.* **2007**, *17*, 1887–1895.
9. Brunner, K.; Dijken, A. van; Börner, H.; Bastiaansen, J. J. A. M.; Kiggen, N. M. M.; Langeveld, B. M. W. *J. Am. Chem. Soc.* **2004**, *126*, 6035–6042.
10. Van Dijken, A.; Bastiaansen, J. J. A. M.; Kiggen, N. M. M.; Langeveld, B. M. W.; Rothe, C.; Monkman, A.; Bach, I.; Stössel, P.; Brunner, K. *J. Am. Chem. Soc.* **2004**, *126*, 7718–7727.
11. Schrögel, P.; Tomkevičienė, A.; Strohriegl, P.; Hoffmann, S. T.; Köhler, A.; Lennartz, C. *J. Mater. Chem.* **2011**, *21*, 2266.
12. Gong, S.; He, X.; Chen, Y.; Jiang, Z.; Zhong, C.; Ma, D.; Qin, J.; Yang, C. *J. Mater. Chem.* **2012**, *22*, 2894–2899.
13. He, J.; Liu, H.; Dai, Y.; Ou, X.; Wang, J.; Tao, S.; Zhang, X.; Wang, P.; Ma, D. *J. Phys. Chem. C* **2009**, *113*, 6761–6767.
14. Oh, C. S.; Lee, C. W.; Lee, J. Y. *Dyes Pigments* **2013**, *98*, 372–376.
15. Ren, X.; Li, J.; Holmes, R. J.; Djurovich, P. I.; Forrest, S. R.; Thompson, M. E. *Chem. Mater.* **2004**, *16*, 4743–4747.
16. Kang, J. W.; Lee, D. S.; Park, H. D.; Kim, J. W.; Jeong, W. I.; Park, Y. S.; Lee, S. H.; Go, K.; Lee, J. S.; Kim, J. J. *Org. Electron.* **2008**, *9*, 452–460.
17. Tsuboi, T.; Liu, S. W.; Wu, M. F.; Chen, C. T. *Org. Electron.* **2009**, *10*, 1372–1377.
18. Gong, S.; Fu, Q.; Wang, Q.; Yang, C.; Zhong, C.; Qin, J.; Ma, D. *Adv. Mater.* **2011**, *23*, 4956–4959.
19. Hu, D.; Cheng, G.; Liu, H.; Lv, Y.; Lu, P.; Ma, Y. *Org. Electron.* **2012**, *13*, 2825–2831.
20. Cho, Y. J.; Lee, J. Y. *J. Phys. Chem. C* **2011**, *115*, 10272–10276.
21. Fan, C.; Chen, Y.; Liu, Z.; Jiang, Z.; Zhong, C.; Ma, D.; Qin, J.; Yang, C. *J. Mater. Chem. C* **2013**, *1*, 463–469.
22. Hu, D.; Lu, P.; Wang, C.; Liu, H.; Wang, H.; Wang, Z.; Fei, T.; Gu, X.; Ma, Y. *J. Mater. Chem.* **2009**, *19*, 6143–6148.
23. Kim, O. Y.; Lee, J. Y. *J. Ind. Eng. Chem.* **2012**, *18*, 1029–1032.
24. Liu, H.; Bai, Q.; Yao, L.; Hu, D.; Tang, X.; Shen, F.; Zhang, H.; Gao, Y.; Lu, P.; Yang, B.; Ma, Y. *Adv. Funct. Mater.* **2014**, *24*, 5881–5888.
25. Tsai, M. H.; Hong, Y. H.; Chang, C. H.; Su, H. C.; Wu, C. C.; Matoliukstyte, A.; Simokaitiene, J.; Grigalevicius, S.; Grazulevicius, J. V.; Hsu, C. P. *Adv. Mater.* **2007**, *19*, 862–866.
26. Sun, J.; Jiang, H.; Zhang, J.; Tao, Y.; Chen, R. *New J. Chem.* **2013**, *37*, 977–985.
27. Tsai, M. H.; Ke, T. H.; Lin, H. W.; Wu, C. C.; Chiu, S. F.; Fang, F. C.; Liao, Y. L.; Wong, K. T.; Chen, Y. H.; Wu, C. I. *ACS Appl. Mater. Interfaces* **2009**, *1*, 567–574.
28. Pommerehne, J.; Vestweber, H.; Guss, W.; Mahrt, R. F.; Bässler, H.; Porsch, M.; Daub, J. *Adv. Mater.* **1995**, *7*, 551–554.
29. Ambrose, J. F.; Carpenter, L. L.; Nelson, R. F. *J. Electrochem. Soc.* **1975**, *122*, 876–894.
30. Chiu, S. K.; Chung, Y. C.; Liou, G. S.; Su, Y. O. *J. Chinese Chem. Soc.* **2012**, *59*, 331–337.
31. Tao, Y.; Gong, S.; Wang, Q.; Zhong, C.; Yang, C.; Qin, J.; Ma, D. *Phys. Chem. Chem. Phys.* **2010**, *12*, 2438–2442.
32. Tomkeviciene, A.; Grazulevicius, J. V; Volyniuk, D.; Jankauskas, V.; Sini, G. *Phys. Chem. Chem. Phys.* **2014**, *16*, 13932–13942.
33. Hirata, S.; Heo, H. J.; Shibano, Y.; Hirata, O.; Yahiro, M.; Adachi, C. *Jpn. J. Appl. Phys.* **2012**, *51*, 041604–041609.
34. Macit, H.; Sen, S.; Sacak, M. *J. Appl. Polym. Sci.* **2005**, *96*, 894–898.
35. Frisch, M. J.; Trucks, G. W.; Schlegel, H. B.; Scuseria, G. E.; Robb, M. A.; Cheeseman, J. R.; Scalmani, G.; Barone, V.; Mennucci, B.; Petersson, G. A.; et al. *Gaussian 09, Revis. C.01,* Gaussian Inc.: Wallingford CT, USA, 2010.
36. Li, Q.; Cui, L. S.; Zhong, C.; Yuan, X. D.; Dong, S. C.; Jiang, Z. Q.; Liao, L. S. *Dyes Pigments* **2014**, *101*, 142–149.
37. Ge, Z.; Hayakawa, T.; Ando, S.; Ueda, M.; Akiike, T.; Miyamoto, H.; Kajita, T.; Kakimoto, M. *Chem. Mater.* **2008**, *20*, 2532–2537.
38. Salert, B. C. D.; Wedel, A.; Grubert, L.; Eberle, T.; Anémian, R.; Krueger, H. *Adv. Mater. Sci. Eng.* **2012**, *2012*, 1–15.

**A tetraphenylsilane group containing carbazoles as high triplet energy host materials for solution-processable PhOLEDs**

Saliha ÖNER, İlker ÖNER**, Haydar AKDAĞ, Canan VARLIKLI
Ege University, Solar Energy Institute, Bornova, İzmir, Turkey

Supplementary (S)

**Synthesis:**

**Synthesis of 3,6-di-*tert*-butylcarbazole (2):** Carbazole (5.01 g, 30 mmol) and $AlCl_3$ (3.99 g, 30 mmol) were weighed into a 250-mL 3-necked round-bottom flask. Dichloromethane (DCM, 100 mL) was added to the flask and the solution was cooled to 0 °C with an ice-water bath. *tert*-Butyl chloride (t-BuCl, 66 mmol, 7.3 mL) was dissolved in DCM (20 mL) and added to the flask dropwise at 0 °C. The resultant solution was left to stir at room temperature (RT) overnight. Next 100 g of cold water was added to the reaction mixture and the organic phase was extracted. The water phase was washed with DCM (50 mL) and the organic phases were combined and dried over $MgSO_4$. After removal of the solvent, the residue was purified by recrystallization from DCM/petroleum ether mixture and pale white solid was obtained. Yield: 54%. IR (500–4000 $cm^{-1}$, KBr pellet): 3415, 2958, 2903, 2864, 1493, 1471, 1392, 1363, 1300, 1264, 1250, 820, 617. $^1$H NMR ($\delta_H$, *ppm*, 400 MHz, $CDCl_3$): 8.07 (s, 2H, Ar); 7.66 (s, 1H, N–H); 7.47–7.42 (d, $J$ = 8.4 Hz, 2H, Ar); 7.25–7.22 (d, $J$ = 8.8 Hz, 2H, Ar); 1.44 (s, 18H).

**Synthesis of bis(4-bromophenyl)(diphenyl)silane (3):** 1,4-dibromobenzene (12 mmol, 2.83 g) was weighed into a 250-mL Schlenk and dissolved in THF (50 mL). The solution was cooled to –78 °C by using a dry ice/acetone mixture. N-butyllithium (*n*-BuLi, 2.5 M in hexane, 14.40 mmol, 5.76 mL) was added dropwise to the Schlenk using a syringe and the solution was stirred at –78 °C for 1 h. After that, dichloro(diphenyl)silane (5 mmol, 1.05 mL) was added to the Schlenk dropwise and the resultant solution was stirred at RT overnight. Water (50 mL) was added to the reaction mixture and the THF phase was extracted. The water phase was washed with DCM (50 mL), and the organic phases collected and dried over $MgSO_4$. After the removal of the solvents, a white solid was obtained and purified by recrystallization from the EtOH. Yield: 51%. IR (500–4000 $cm^{-1}$, KBr pellet): 3065, 3024, 1567, 1549, 1477, 1428, 1376, 1301, 1183, 1111, 1062, 1008, 998, 809, 728, 711, 698, 537, 522, 512. $^1$H NMR ($\delta_H$, *ppm*, 400 MHz, $CDCl_3$): 7.60–7.52 (m, 8H, Ar); 7.47–7.35 (m, 10H, Ar).

**Synthesis of 9,9'-[(diphenylsilanediyl)bis(4,1-phenylene)]bis-*9H*-carbazole [DiCzSi]:** Carbazole (4 mmol, 0.67 g), bis(4-bromophenyl)(diphenyl)silane (2) (2 mmol, 0.99 g), and $K_2CO_3$ (8 mmol, 1.10 g) were weighed into a 50-mL 2-necked round-bottom flask equipped with a reflux condenser. Toluene (20 mL) was added to the reaction flask and degassed by argon for 20 min. Pd(OAc) (0.08 mmol, 18 mg) and P(t-Bu)$_3$ (0.32 mmol, 65 mg) were weighed in a glovebox and transferred to the reaction flask. The

resultant mixture was heated to 80 °C overnight. After cooling, EtOAc (20 mL) was added to the mixture and the insoluble solid was removed by filtering. Solvents were removed by rotary evaporator and the crude product was purified by column chromatography from the hexane/DCM (10/1) solvent system. Yield: 38%. Mp: 290 °C. IR (500–4000 $cm^{-1}$, KBr pellet): 3049, 3023, 1624, 1618, 1591, 1506, 1478, 1450, 1428, 1361, 1334, 1317, 1228, 1173, 1111, 1096, 1017, 999, 915, 826, 765, 748, 722, 700, 676, 525, 536, 520. $^{1}$H NMR ($\delta_H$, *ppm,* 400 MHz, $CDCl_3$): 8.19–8.16 (d, *J* = 8.4 Hz, 4H, Ar); 7.93–7.89 (d, *J* = 8.4 Hz, 4H, Ar); 7.78–7.75 (d, *J* = 8.0 Hz, 4H, Ar); 7.70–7.67 (d, *J* = 8.4 Hz, 4H, Ar); 7.57–7.43 (m, 14H, Ar); 7.34–7.30 (t, *J* = 7.6 Hz, 4H, Ar). $^{13}$C NMR ($\delta_C$, *ppm*, 400 MHz, $CDCl_3$): 140.59; 139.26; 137.92; 136.45; 133.59; 133.20; 130.05; 128.21; 126.29; 125.97; 123.59; 120.34; 120.14; 109.91. MS (+FAB) m/z: 666.3 (M+H).

**Synthesis of 9,9'-[(diphenylsilanediyl)bis(4,1-phenylene)]bis(3,6-di-*tert*-butyl-*9H*-carbazole) [tBuDiCzSi]:** 3,6-di-*tert*-butylcarbazole (1) (4 mmol, 1.12 g), bis(4-bromophenyl)(diphenyl)silane (2) (2 mmol, 0.99 g), and $K_2CO_3$ (8 mmol, 1.10 g) were weighed into a 25-mL 2-necked round-bottom flask equipped with a reflux condenser. Toluene (20 mL) was added to the reaction flask and degassed by argon for 20 min. Pd(OAc) (0.08 mmol, 18 mg) and P(t-Bu)$_3$ (0.32 mmol, 65 mg) were weighed in a glovebox and transferred to the reaction flask. The resultant mixture was heated to 80 °C overnight. After cooling, EtOAc (20 mL) was added to the mixture and the insoluble solid was removed by filtering. Solvents were removed by rotary evaporator and the crude product was purified by column chromatography from the hexane/DCM (10/1) solvent system. Yield: 45%. Mp: 384 °C. IR (500–4000 $cm^{-1}$, KBr pellet): 2958, 1592, 1488, 1470, 1363, 1324, 1292, 1262, 1232, 1179, 1111, 1077, 880, 840, 807, 739, 703, 537. $^{1}$H NMR ($\delta_H$, *ppm,* 400 MHz, $CDCl_3$): 8.26 (s, 4H, Ar); 7.99–7.95 (d, *J* = 7.6 Hz, 4H, Ar); 7.86–7.82 (d, *J* = 8.0 Hz, 4H, Ar); 7.78–7.74 (d, *J* = 8.4 Hz, 4H, Ar); 7.62–7.54 (m, 14H, Ar); 1.57 (s, 36H). $^{13}$C NMR (δH, ppm, 400 MHz, $CDCl_3$): 145.79; 143.22; 139.93; 139.11; 138.01; 136.63; 133.93; 132.70; 130.17; 128.36; 126.02; 123.81; 116.43; 109.59; 34.91; 32.21. MS (+FAB) m/z: 890.7 (M+H).

**Synthesis of 9-(4-bromophenyl)-*9H*-carbazole (4):** Carbazole (10 mmol, 1.67 g), 1-bromo-4-iodobenzene (12 mmol, 3.40 g), Cu (10 mmol, 0.64 g), 18-Crown-6 (2 mmol, 0.53 g), and $K_2CO_3$ (20 mmol, 2.76 g) were weighed into a 100-mL 2-necked round-bottom flask equipped with a reflux condenser. DMF (50 mL) was added to the reaction flask and the resultant mixture was heated to reflux overnight. After cooling, 100 mL of cold water was poured onto the reaction mixture and a yellow precipitate was obtained. The solid material was filtered under vacuum and the crude product was purified by column chromatography from the hexane/DCM (10/1) solvent system. Yield: 62%. IR (500–4000 $cm^{-1}$, KBr pellet): 3040, 2927, 1596, 1584, 1497, 1479, 1453, 1363, 1335, 1316, 1231, 1181, 1121, 1100, 1067, 1009, 827, 750, 726, 709. $^{1}$H NMR ($\delta_H$, *ppm,* 400 MHz, $CDCl_3$): 8.18–8.15 (d, *J* = 8.4 Hz, 2H, Ar); 7.76–7.73 (d, *J* = 8.4 Hz, 2H, Ar); 7.50–7.30 (m, 8H, Ar).

**Synthesis of 9-(4-bromophenyl)-3,6-di-*tert*-butyl-*9H*-carbazole (5):** 3,6-di-*tert*-butylcarbazole (1) (6 mmol, 1.67 g), 1-bromo-4-iodobenzene (7.5 mmol, 2.12 g), Cu (10 mmol, 0.64 g), 18-Crown-6 (2 mmol, 0.53 g), and $K_2CO_3$ (20 mmol, 2.76 g) were weighed into a 100-mL 2-necked round-bottom flask equipped with a reflux condenser. DMF (50 mL) was added to the reaction flask and the resultant mixture

was heated to reflux overnight. After cooling, 100 mL of cold water was poured onto the reaction mixture and a yellow precipitate was formed. The solid material was filtered under vacuum and the crude product was purified by column chromatography from the hexane/DCM (10/1) solvent system. Yield: 62%. IR (500–4000 $cm^{-1}$, KBr pellet): 3040, 2927, 1596, 1584, 1497, 1479, 1453, 1363, 1335, 1316, 1231, 1181, 1121, 1100, 1067, 1009, 827, 750, 726, 709. $^1$H NMR ($\delta_H$, *ppm,* 400 MHz, $CDCl_3$): 8.17 (s, 2H, Ar); 7.91–7.89 (d, $J$ = 8.4 Hz, 2H, Ar); 7.70–7.68 (d, $J$ = 8.4 Hz, 2H, Ar); 7.52–7.44 (m, 4H, Ar); 1.49 (s, 18H).

**Synthesis of [4-(*9H*-carbazol-9-yl)phenyl]boronic acid (6):** 9-(4-bromophenyl)-3,6-di-*tert*-butyl-*9H*-carbazole (5) (1 mmol, 0.32 g) was added to a 50-mL 2-necked round-bottom flask and dissolved in THF (20 mL). The solution was cooled to –78 °C by using dry ice/acetone mixture. After cooling, *n*-BuLi (2.5 M in hexane, 5 mmol, 2 mL) was added to the flask dropwise and the solution was stirred at –78 °C for 1 h. Trimethylborate (5 mmol, 0.56 mL) was added to the flask dropwise and the resultant solution was stirred at RT overnight. Then 50 mL of cold water was added to the reaction mixture and the THF phase was separated. The water phase was washed with DCM (50 mL), and the organic phases collected and dried over $MgSO_4$. After removal of the solvents, a white solid was precipitated from the hexane/EtOAc mixture. Yield: 44%. IR (500–4000 $cm^{-1}$, KBr pellet): 3212, 1604, 1559, 1479, 1451, 1412, 1353, 1221, 1196, 1169, 1109, 1016, 741, 719, 692.

**Synthesis of [4-(3,6-di-*tert*-butyl-*9H*-carbazol-9-yl)phenyl]boronic acid (7):** 9-(4-bromophenyl)-3,6-di-*tert*-butyl-*9H*-carbazole (7) (4 mmol, 1.74 g) was added to a 100-mL 2-necked round-bottom flask and dissolved in THF (50 mL). The solution was cooled to –78 °C by using dry ice/acetone mixture. After cooling, *n*-BuLi (2.5 M in hexane, 6 mmol, 2.40 mL) was added to the flask dropwise and the solution was stirred at –78 °C for 1 h. Trimethylborate (8 mmol, 0.89 mL) was added to the flask dropwise and the resultant solution was stirred at RT overnight. Then 50 mL of cold water was added to the reaction mixture and the THF phase was separated. The water phase was washed with DCM (50 mL), and the organic phases collected and dried over $MgSO_4$. After removal of the solvents, a white solid was precipitated from the hexane. Yield: 48%. IR (500–4000 $cm^{-1}$, KBr pellet): 2960, 2904, 2866, 1602, 1560, 1489, 1473, 1420, 1406, 1345, 1324, 1297, 1262, 1232, 1175, 1106, 1083, 878, 842, 812, 752, 741, 708, 692.

**Synthesis of 9,9'-[(diphenylsilanediyl)bis(biphenyl-4',4-diyl)]bis-*9H*-carbazole [DiCzPhSi]:** [4-(*9H*-carbazol-9-yl)phenyl]boronic acid (6) (1 mmol, 0.29 g), bis(4-bromophenyl)(diphenyl)silane (2) (0.4 mmol, 0.2 g), $Cs_2CO_3$ (2 mmol, 0.65 g), and Pd(dppf)$Cl_2$ (0.08 mmol, 65 mg) were weighed in a 25-mL 2-necked round-bottom flask equipped with a reflux condenser. Toluene/MeOH (10/5 mL) solvent mixture was added to the reaction flask and argon gas was bubbled through the solution for about 20 min. The resultant solution was heated to 80 °C overnight. After cooling, EtOAc (20 mL) was added to the mixture and the insoluble solid was removed by filtering. Solvents were removed by rotary evaporator and the crude product was purified by column chromatography from the hexane/DCM (10/1) solvent system. Yield: 42%. Mp: 285 °C. IR (500–4000 $cm^{-1}$, KBr pellet): 3035, 1597, 1521, 1493, 1451, 1426, 1364, 1334, 1315, 1228, 1184, 1110, 1004, 816, 752, 723, 712, 626, 559, 531, 521. $^1$H NMR ($\delta_H$, *ppm,* 400 MHz, $CDCl_3$): 8.19–8.15 (d, $J$ = 8.0 Hz, 4H, Ar); 7.88–7.85 (d, $J$ = 8.4 Hz, 4H, Ar); 7.80–7.74 (m,

8H, Ar); 7.72–7.65 (m, 8H, Ar); 7.52–7.42 (m, 14H, Ar); 7.34–7.30 (t, $J$ = 6.8 Hz, 4H, Ar). $^{13}$C NMR (δH, ppm, 400 MHz, $CDCl_3$): 141.36; 140.84; 139.91; 137.17; 137.06; 136.44; 134.03; 133.47; 129.80; 128.51; 128.03; 127.37; 126.60; 125.97; 123.47; 120.32; 120.01; 109.83. MS (+FAB) m/z: 818.4 (M+H).

**Synthesis of 9,9'-[(diphenylsilanediyl)bis(biphenyl-4',4-diyl)]bis(3,6-di-*tert*-butyl-*9H*-carbazole) [tBuDiCzPhSi]:** [4-(3,6-di-*tert*-butyl-*9H*-carbazol-9-yl)phenyl]boronic acid (8) (1 mmol, 0.4 g), bis(4-bromophenyl)(diphenyl)silane (2) (0.4 mmol, 0.2 g), $Cs_2CO_3$ (2 mmol, 0.65 g), and Pd(dppf)$Cl_2$ (0.08 mmol, 65 mg) were weighed in a 25-mL 2-necked round-bottom flask equipped with a reflux condenser. Toluene/MeOH (10/5 mL) solvent mixture was added to the reaction flask and argon gas was bubbled through the solution for about 20 min. The resultant solution was heated to 80 °C overnight. After cooling, EtOAc (20 mL) was added to the mixture and the insoluble solid was removed by filtering. Solvents were removed by rotary evaporator and the crude product was purified by column chromatography from the hexane/DCM (10/1) solvent system. Yield: 56%. Mp: na. IR (500–4000 $cm^{-1}$, KBr pellet): 3042, 2952, 2907, 2862, 1603, 1522, 1491, 1473, 1364, 1324, 1294, 1261, 1233, 1190, 1111, 1004, 879, 810, 769, 725, 699, 611, 530, 511. $^1$H NMR ($\delta_H$, *ppm,* 400 MHz, $CDCl_3$): 8.18 (s, 4H, Ar); 7.87–7.84 (d, $J$ = 8.4 Hz, 4H, Ar); 7.81–7.75 (m, 8H, Ar); 7.74–7.71 (m, 4H, Ar); 7.69–7.65 (m, 4H, Ar); 7.54–7.43 (m, 14H, Ar); 1.50 (s, 36H). $^{13}$C NMR (δH, ppm, 400 MHz, $CDCl_3$): 142.96; 141.45; 139.36; 139.20; 137.70; 137.06; 136.46; 134.10; 133.35; 129.79; 128.39; 128.03; 126.96; 126.57; 123.63; 123.48; 116.25; 109.29; 34.74; 32.03. MS (+FAB) m/z: 1043.6 (M+H).

## $^{1}$H NMR and $^{13}$C NMR Spectra

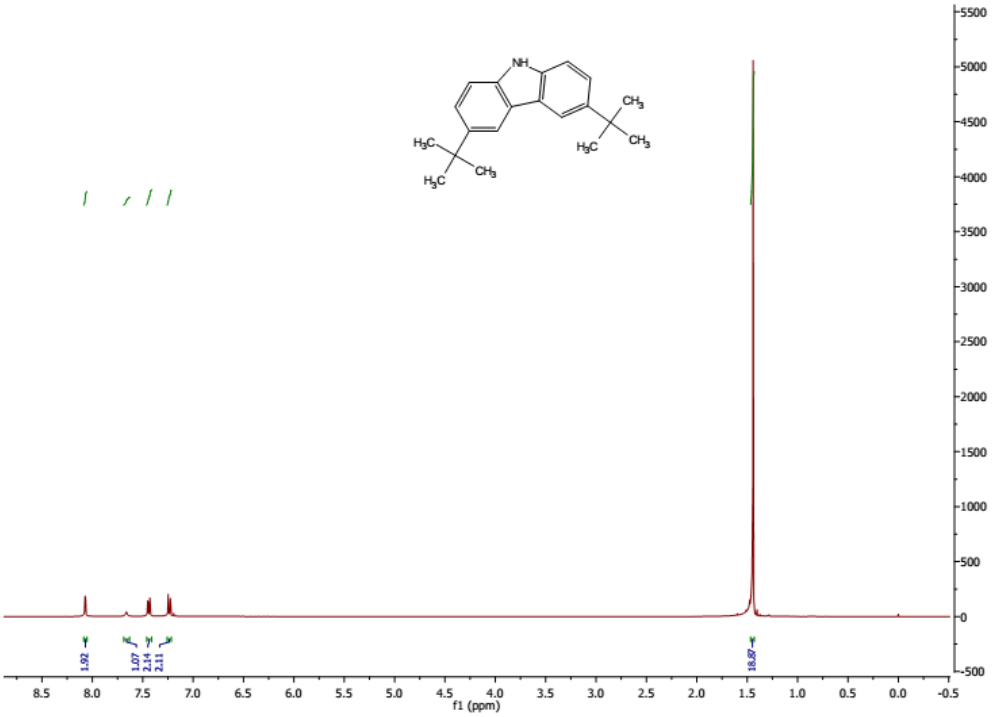


**Figure S1.** $^{1}$H NMR spectrum of 3,6-di-*tert*-butylcarbazole (2).

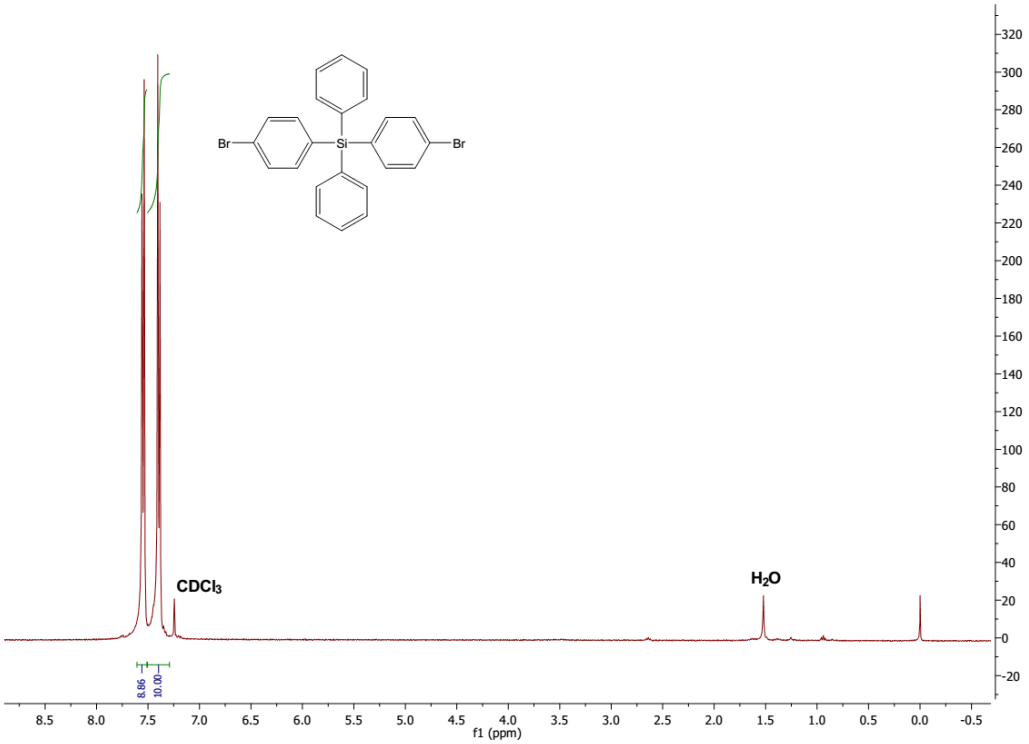


**Figure S2.** $^{1}$H NMR spectrum of bis(4-bromophenyl)(diphenyl)silane (3).

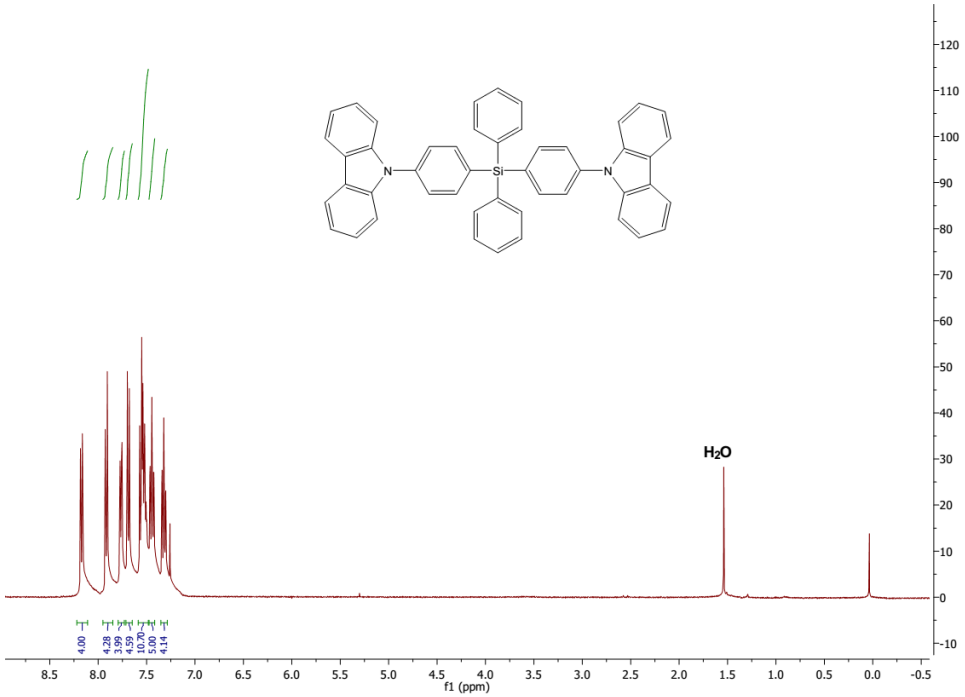


**Figure S3.** $^{1}$H NMR spectrum of 9,9'-[(diphenylsilanediyl)bis(4,1-phenylene)]bis-*9H*-carbazole [DiCzSi].

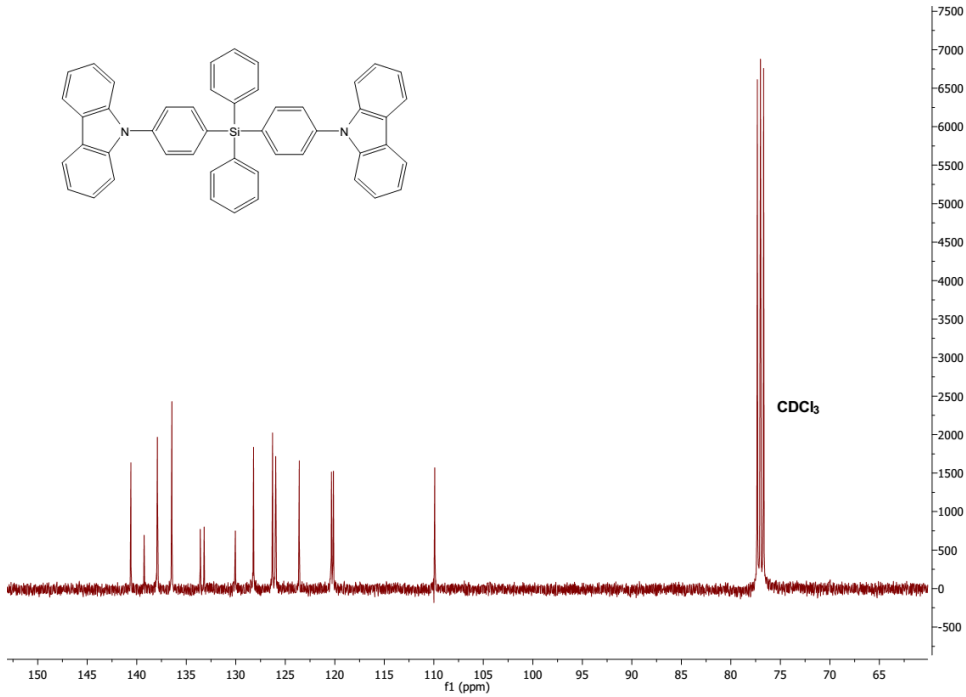


**Figure S4.** $^{13}$C NMR spectrum of 9,9'-[(diphenylsilanediyl)bis(4,1-phenylene)]bis-*9H*-carbazole [DiCzSi].

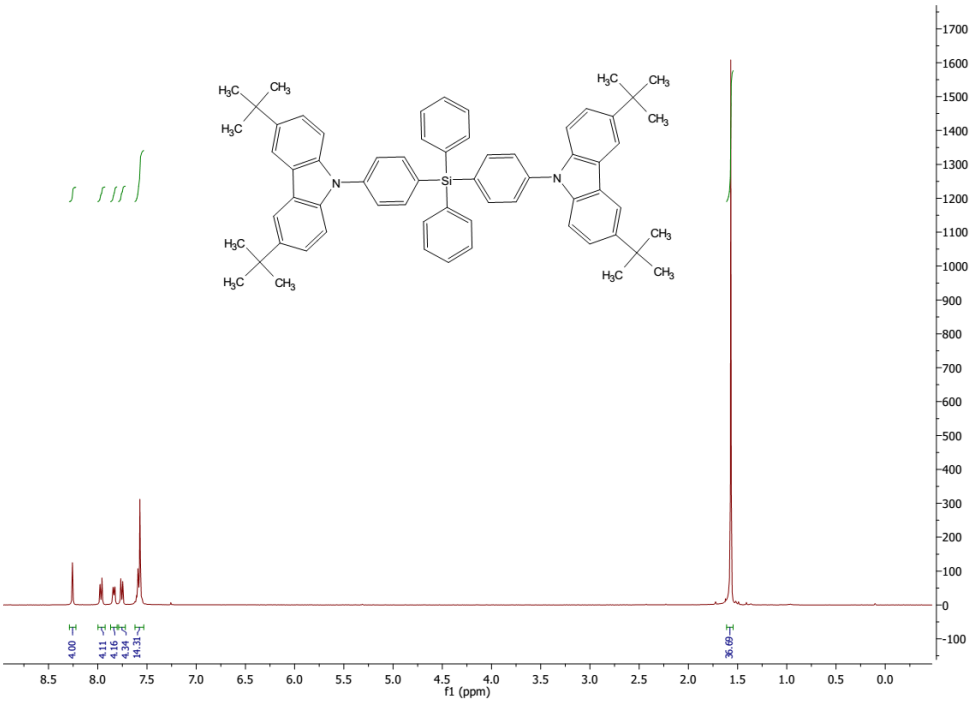


**Figure S5.** [1]H NMR spectrum of 9,9'-[(diphenylsilanediyl)bis(4,1-phenylene)]bis(3,6-di-*tert*-butyl-*9H*-carbazole) [tBuDiCzSi].

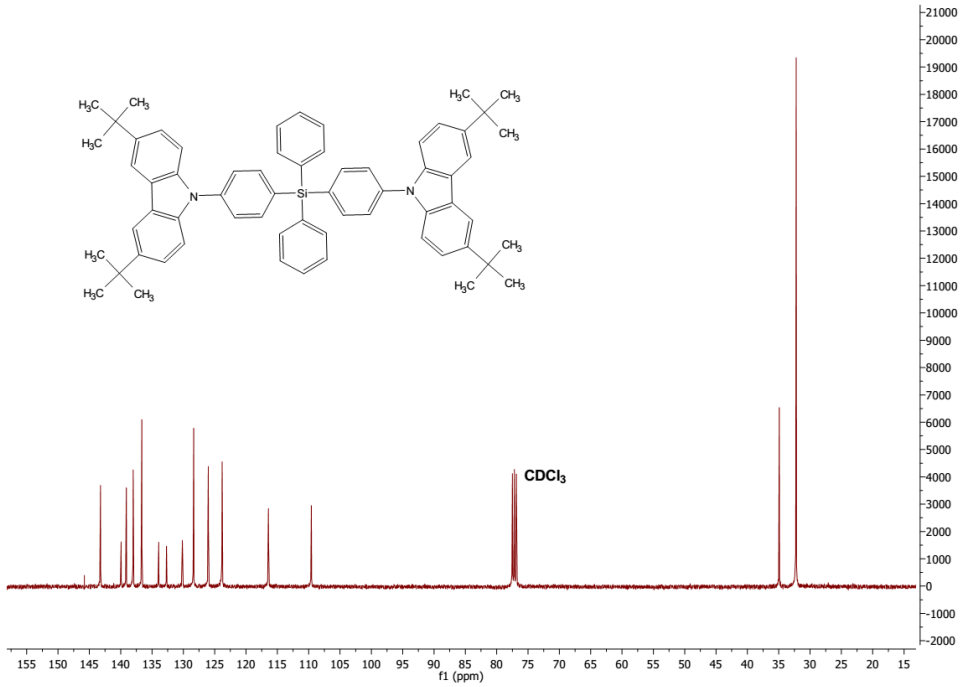


**Figure S6.** [13]C NMR spectrum of 9,9'-[(diphenylsilanediyl)bis(4,1-phenylene)]bis(3,6-di-*tert*-butyl-*9H*-carbazole) [tBuDiCzSi].

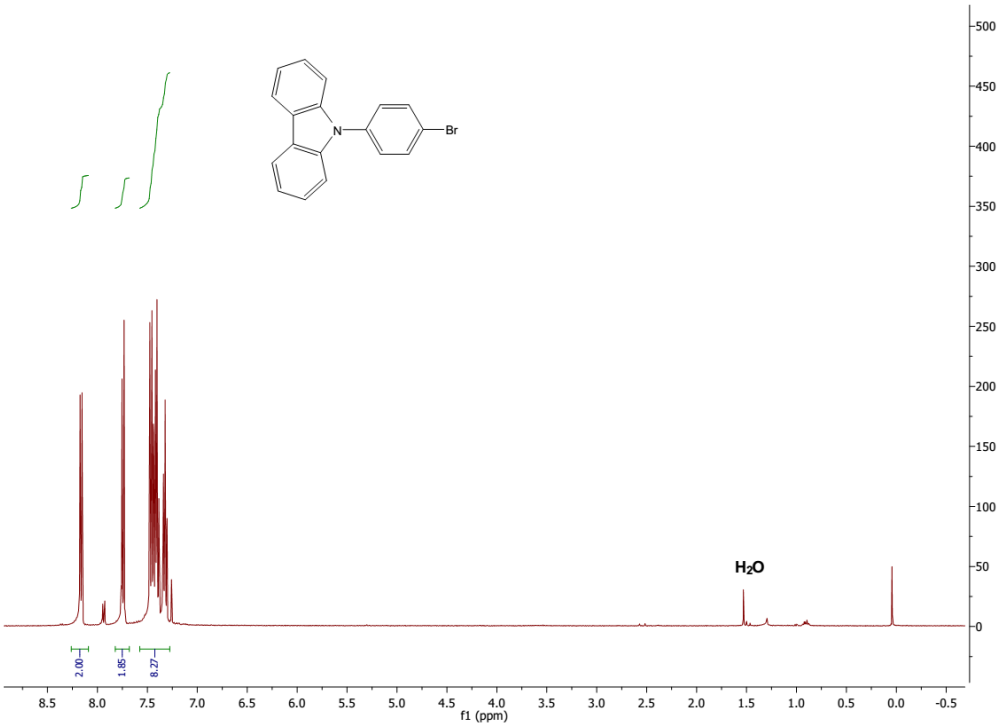


**Figure S7.** $^{1}$H NMR spectrum of 9-(4-bromophenyl)-*9H*-carbazole (4).

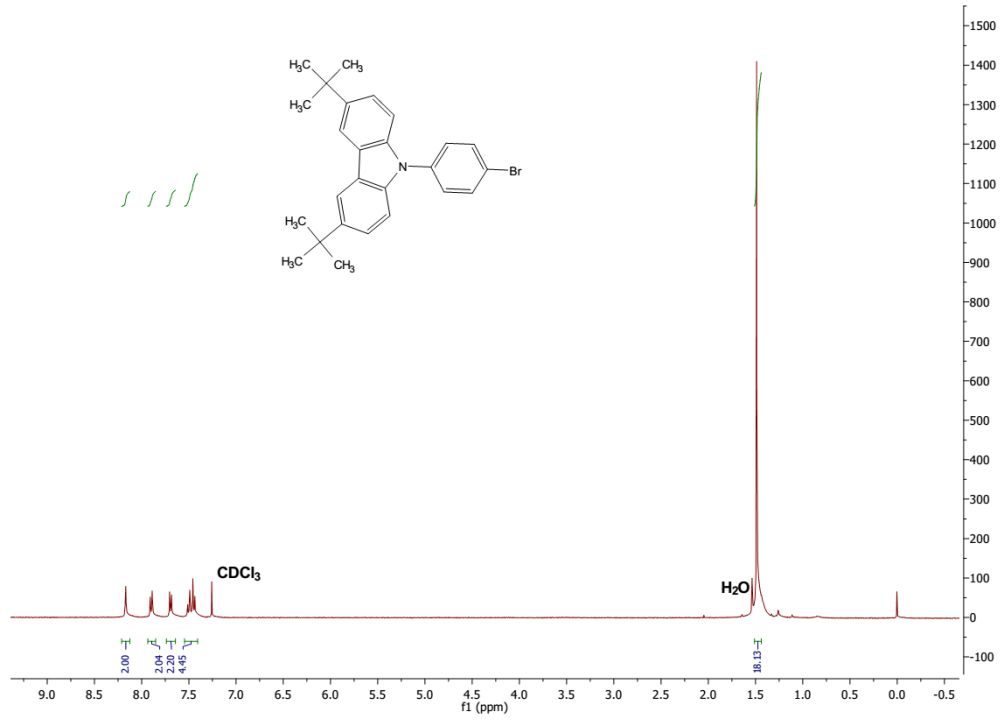


**Figure S8.** $^{1}$H NMR spectrum of 9-(4-bromophenyl)-3,6-di-*tert*-butyl-*9H*-carbazole (5).

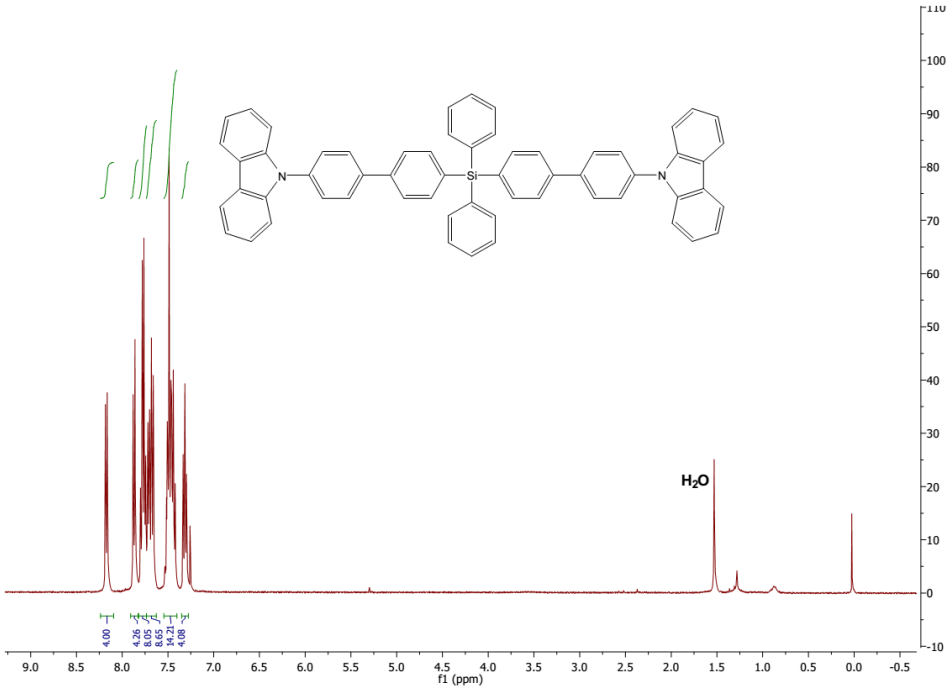


**Figure S9.** $^{1}$H NMR spectrum of 9,9'-[(diphenylsilanediyl)bis(biphenyl-4',4-diyl)]bis-*9H*-carbazole [DiCzPhSi].

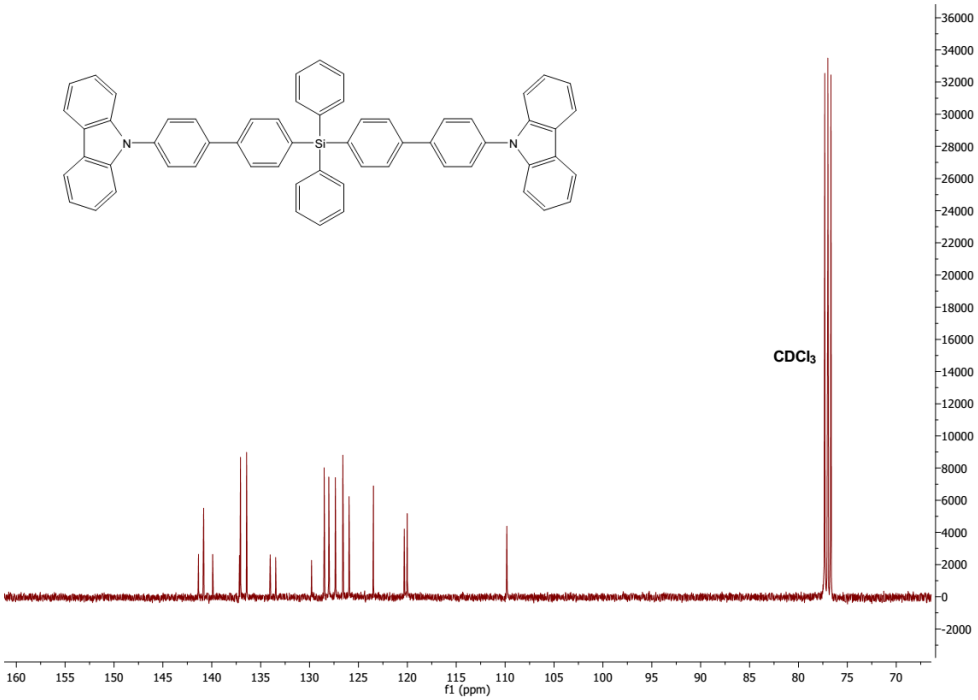


**Figure S10.** $^{13}$C NMR spectrum of 9,9'-[(diphenylsilanediyl)bis(biphenyl-4',4-diyl)]bis-*9H*-carbazole [DiCzPhSi].

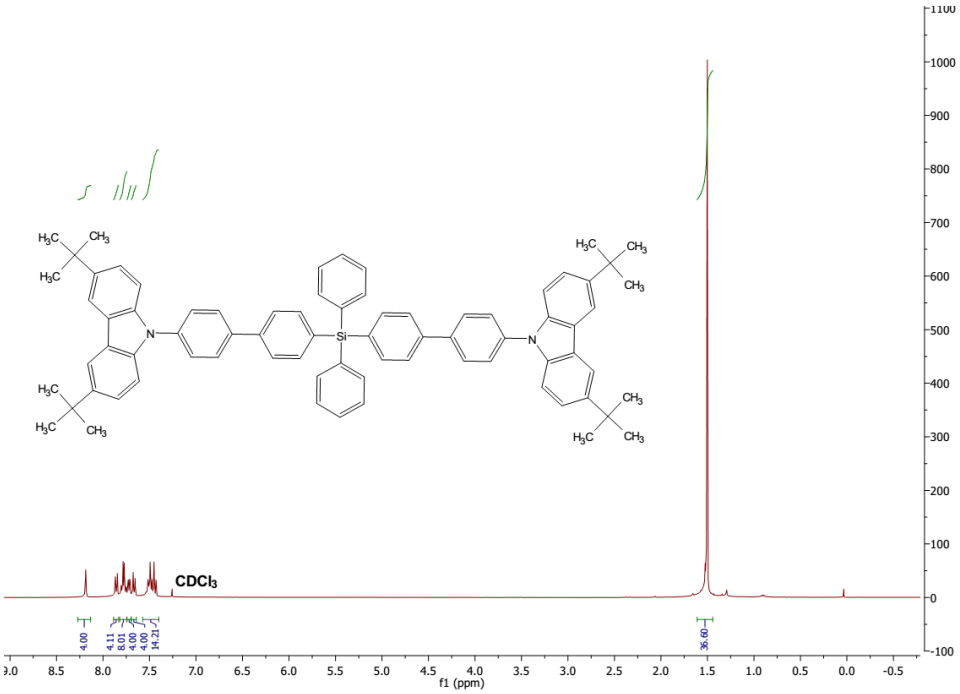


**Figure S11.** $^{1}$H NMR spectrum of 9,9'-[(diphenylsilanediyl)bis(biphenyl-4',4-diyl)]bis(3,6-di-*tert*-butyl-*9H*-carbazole) [tBuDiCzPhSi].

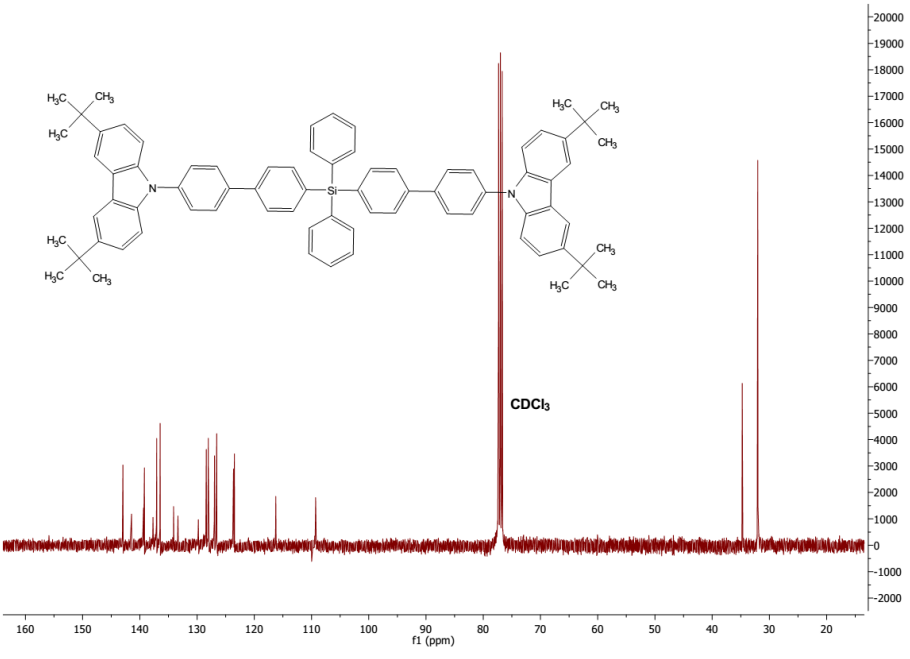


**Figure S12.** $^{13}$C NMR spectrum of 9,9'-[(diphenylsilanediyl)bis(biphenyl-4',4-diyl)]bis(3,6-di-*tert*-butyl-*9H*-carbazole) [tBuDiCzPhSi].

**Electrochemical stability**

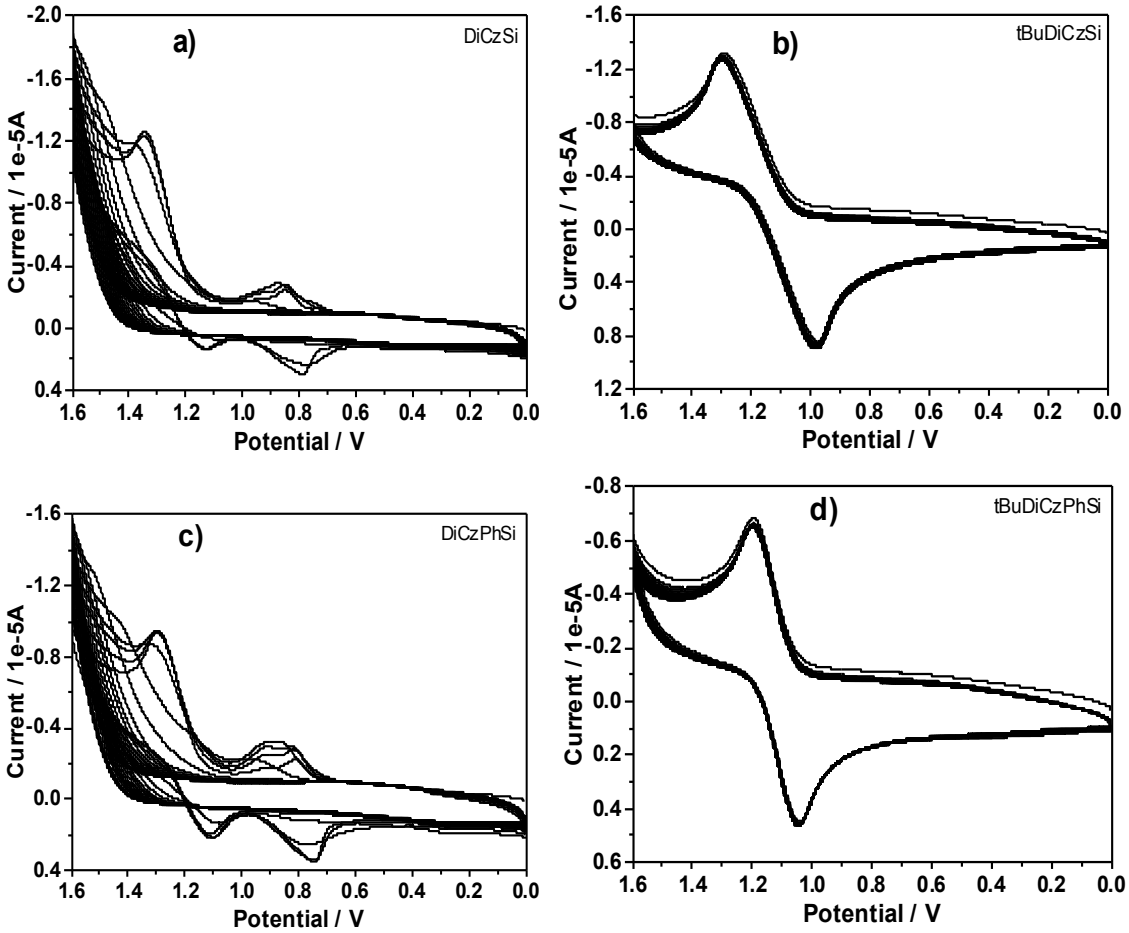


**Figure S13.** Consecutive cyclic voltammograms (20 cycles) of the synthesized materials, a) DiCzSi, b) tBuDiCzSi, c) DiCzPhSi, and d) tBuDiCzPhSi measured in $CHCl_3$.